SANDIA REPORT
SAND2013-2690
Unlimited Release
Printed April 2013

Integration of MHD load models with circuit representations the Z generator

Chris A. Jennings, David J. Ampleford, Brent M. Jones, Ryan D. McBride, James E. Bailey, Michael C. Jones, Matthew R. Gomez, Mike E. Cuneo, Charles Nakhleh, William. A. Stygar, Mark Savage, Tim C. Wagoner, James. K. Moore

Prepared by
Sandia National Laboratories
Albuquerque, New Mexico 87185 and Livermore, California 94550

Sandia National Laboratories is a multi-program laboratory managed and operated by Sandia Corporation, a wholly owned subsidiary of Lockheed Martin Corporation, for the U.S. Department of Energy's National Nuclear Security Administration under contract DE-AC04-94AL85000.

Approved for public release; further dissemination unlimited.

Sandia National Laboratories

Issued by Sandia National Laboratories, operated for the United States Department of Energy by Sandia Corporation.

NOTICE: This report was prepared as an account of work sponsored by an agency of the United States Government. Neither the United States Government, nor any agency thereof, nor any of their employees, nor any of their contractors, subcontractors, or their employees, make any warranty, express or implied, or assume any legal liability or responsibility for the accuracy, completeness, or usefulness of any information, apparatus, product, or process disclosed, or represent that its use would not infringe privately owned rights. Reference herein to any specific commercial product, process, or service by trade name, trademark, manufacturer, or otherwise, does not necessarily constitute or imply its endorsement, recommendation, or favoring by the United States Government, any agency thereof, or any of their contractors or subcontractors. The views and opinions expressed herein do not necessarily state or reflect those of the United States Government, any agency thereof, or any of their contractors.

Printed in the United States of America. This report has been reproduced directly from the best available copy.

Available to DOE and DOE contractors from
U.S. Department of Energy
Office of Scientific and Technical Information
P.O. Box 62
Oak Ridge, TN 37831

Telephone: (865) 576-8401
Facsimile: (865) 576-5728
E-Mail: reports@adonis.osti.gov
Online ordering: http://www.osti.gov/bridge

Available to the public from
U.S. Department of Commerce
National Technical Information Service
5285 Port Royal Rd.
Springfield, VA 22161

Telephone: (800) 553-6847
Facsimile: (703) 605-6900
E-Mail: orders@ntis.fedworld.gov
Online order: http://www.ntis.gov/help/ordermethods.asp?loc=7-4-0#online

SAND2013-2690
Unlimited Release
Printed April 2013

Integration of MHD load models with circuit representations the Z generator

Chris A. Jennings, David J. Ampleford, Brent M. Jones, Ryan D. McBride, James E. Bailey, Michael C. Jones, Matthew R. Gomez, Mike E. Cuneo, Charles Nakhleh, William. A. Stygar, Mark Savage, Tim C. Wagoner, James. K. Moore
Sandia National Laboratories
P.O. Box 5800
Albuquerque, New Mexico 87185-MS1106

Abstract

MHD models of imploding loads fielded on the Z accelerator are typically driven by reduced or simplified circuit representations of the generator. The performance of many of the imploding loads is critically dependent on the current and power delivered to them, so may be strongly influenced by the generators response to their implosion. Current losses diagnosed in the transmission lines approaching the load are further known to limit the energy delivery, while exhibiting some load dependence. Through comparing the convolute performance of a wide variety of short pulse Z loads we parameterize a convolute loss resistance applicable between different experiments. We incorporate this, and other current loss terms into a transmission line representation of the Z vacuum section. We then apply this model to study the current delivery to a wide variety of wire array and MagLif style liner loads.

ACKNOWLEDGMENTS

It is the nature of this analysis that use has been made of a wide variety of data collected on Z. The author would like to gratefully acknowledge:

Principle Investigators – whose data we use in our comparisons:
David Ampleford, Brent Jones, Ryan McBride, Jim Bailey, Michael Jones, Tom Awe, Matt Gomez, Dan Sinars, Mike Cuneo

Simulation people – for data and guidance on load calculations:
Stephanie Hansen, Kyle Cochrane

Hardware designers - for providing information on experimental configurations:
Thomas Strizic, Grafton Robertson

Z People – For making the experiments a success and for the high quality electrical data that constrains our calculations:
W. Stygar, Mark Savage, Jean-Paul Davis, T.C. Wagoner, J.K. Moore

The research described here was funded by Sandia LDRD project number #155458, as an early career LDRD. The authors would like to thank the LDRD program for providing the funding that made this work possible, and Dawn Flicker for support in the proposal of this project.

The authors would like to thank Z operations, diagnostics, engineering, and load hardware for invaluable and dedicated technical assistance that make the experiments performed on Z so successful.

CONTENTS

1. Introduction 11

2. Background 13
   2.1. Z architecture and Terminology 13
   2.2. Why details about the current delivery matter to the load 15
   2.3. Present understanding of the causes of convolute loss 16

3. Representing the Z GENERATOR 17
   3.1. Vacuum Lines 17
   3.2. Insulator Stack 19

4. Characterization of the convolute loss 21
   4.1. The Measured Convolute Loss on Z Experiments 23
      4.1.1. Large diameter (70mm), low mass stainless steel arrays. 25
      4.1.2. Higher mass 65mm diameter stainless steel arrays. 26
      4.1.3. 65mm Nested tungsten wire arrays. 28
      4.1.4. 65mm Nested Copper wire arrays. 29
      4.1.5. Large diameter (50mm), low mass Aluminum arrays. 31
      4.1.6. Dynamic Hohraums. 32
      4.1.7. MagLif style liners 35
      4.1.8. 8cm diameter Krypton gas puff 38
   4.2. Constructing a Generic Convolute Loss 40

5. Application to modeling loads on z 43
   5.1. Low mass 70mm stainless steel wire arrays 45
   5.2. 65mm Stainless Steel Load 46
   5.3. 65mm Copper load 49
   5.4. 50mm Aluminum Load 50
   5.5. 40mm Dynamic Hohlraum Load 51
   5.6. Correlation of feed loss performance with hardware geometry 52
   5.7. MagLif Beryllium Liners 52
   5.7. Gas Puffs 58

6. Conclusions 61

References 63

Appendix - Coupling of Circuit Model to MHD code 67

FIGURES

Figure 1. Central ~2m radius of the Z generator. 14
Figure 2. Stack and Convolute B-dot measurement for large diameter stainless steel load..... 14
Figure 3. Current and Kinetic Energy for Large Diameter Stainless Steel Wire Array 16
Figure 4. Scaled Profiles of the MITL's, and diagram of the insulator stack 18
Figure 5. Capacitance and inductance per unit length. nF/m and nH/m..... 19
Figure 6. Multiple current and voltage measurements at different azimuthal locations in the stack (Z shot 2235)..... 22
Figure 7. Average translated voltage compared to translated average voltage for the A level ... 23
Figure 8. Convolute current and voltage measurement locations..... 24
Figure 9. Translated Stack Current / Convolute Current and Convolute Voltage 25
Figure 10. Convolute resistance with normalized total x-ray power pulse..... 26
Figure 11. Translated Stack Current / Convolute Current and Convolute Voltage 27
Figure 12. Convolute resistance with normalized total x-ray power pulse..... 27
Figure 13. Translated Stack Current / Convolute Current and Convolute Voltage 28
Figure 14. Convolute resistance with normalized total x-ray power pulse..... 29
Figure 15. Translated Stack Current / Convolute Current and Convolute Voltage 30
Figure 16. Convolute resistance with normalized total x-ray power pulse..... 30
Figure 17. Convolute resistance with normalized total x-ray power pulses for two different array masses 31
Figure 18. Translated Stack Current / Convolute Current and Convolute Voltage 32
Figure 19. Convolute resistance with normalized total x-ray power pulse..... 32
Figure 20. Translated Stack Current / Convolute Current and Convolute Voltage 34
Figure 21. Convolute resistance with normalized total x-ray power pulse..... 35
Figure 22. Translated Stack Current / Convolute Current and Convolute Voltage for Z2105.... 36
Figure 23. Convolute resistance Z2105 37
Figure 24. Translated Stack Current / Convolute Current and Convolute Voltage for raised feed 37
Figure 25. Convolute resistance for raised feed..... 38
Figure 26. Translated Stack Current / Convolute Current and Convolute Voltage for Kr gas puff 39
Figure 27. Convolute resistance and normalized total power for Kr gas puff..... 39
Figure 28. Convolute resistances for dynamic hohraum, 70mm stainless, 50mm Aluminium and 65mm stainless loads 40
Figure 29. Onset of convolute loss 41
Figure 30. Convolute voltages corresponding to convolute losses..... 41
Figure 31. Typical density plots for the implosion of large diameter stainless steel wire array. . 43
Figure 32. Convolute and feed section 44
Figure 33. Current Comparison for stainless steel 70mm shot Z2236 46
Figure 34. Current Comparison for stainless steel 65mm shot Z1860 47
Figure 35. Current Comparison with additional feed loss stainless steel 65mm shot Z1860..... 47
Figure 36. Density profiles 2D vs. 3D 48
Figure 37. Comparison of currents between 2D (blue) and 3D (red) 48

Figure 38. Comparison of currents Z1975 Copper Array 50
Figure 39. Comparison of currents Z2337 Aluminium Array 51
Figure 40. Comparison of currents for dynamic hohlraum loads 51
Figure 41. Feed loss profile compared to convolute loss scaling factor 52
Figure 42. Liner driven with measured convolute loss 53
Figure 43. Voltage driven liner calculation 54
Figure 44. Reconstructed convolute resistance (blue), measured resistance (black), dynamic hohlraum resistance (red) 55
Figure 45. High initial inductance liner calculation using measured convolute loss 56
Figure 46. High initial inductance liner calculation using standard convolute loss 56
Figure 47. High initial inductance liner voltage using standard convolute loss 57
Figure 48. Stack and convolute current and voltage measurements for lower (red) and higher (black) inductance liner feeds 58
Figure 49. Current delivery to Kr gas puff 59
Figure 50. Gas puff connection to convolute 60

1. INTRODUCTION

The Z generator [8] is able to deliver up to 27MA in ~100ns. It is routinely used to drive a wide variety of loads, from radiation sources, to potential liner fusion schemes, to dynamic materials experiments.

The performance of many of the imploding wire array, liner, and dynamic material loads driven by Z generator is critically dependent on the current and power that can successfully be delivered to them. To accurately reproduce the performance of many of the loads that have been fielded therefore requires a detailed understanding of, and ability to model:

1) The load itself
2) The response of the generator to the imploding load.
3) Current losses that are both diagnosed, and inferred in the transmission lines that supply current to the load.

Each of these areas represents a significant field of research in its own right, but to date much of the progress has been made by either coupling state of the art MHD models to reduced circuit representations of the generator [13,3,10,11,12], or by coupling more complete generator models to simplified representations of the loads [1,5,6,7,8]. While this has been very successful in developing our understanding, and ability to model each of these components, we are now in a position to advance our understanding in all of these areas by leveraging the knowledge now available and studying the performance of these loads within an integrated load / generator model.

Integration of these system models is necessary for a number of reasons.

1) It has been shown that to effectively reproduce the plasma conditions seen in wire array experiments requires fully 3-dimensional calculations of the load region. Furthermore, the current distribution obtained in these calculations is dependent on the 3 dimensional nature of the imploding plasma [13]. This will affect the inductance, and hence the electrical response of these loads, so will determine how effectively the generator can continue to couple energy to them. These effects may not be adequately reproduced in 1 or 2 dimensional representations of the load.

2) X-ray generating imploding loads can produce x-ray power pulses a few ns in duration through which electrical power may be continually delivered and radiated [2]. The energy available to continue to deliver electrical power to these loads is therefore sourced from a finite volume of the transmission lines, limited by the propagation time. Adequately representing energy delivered during the final stages of implosion therefore requires use of a transmission line circuit model able to resolve these finite propagation time effects.

3) Current losses in the double post hole convolute that joins together the transmission lines feeding the load region have been extensively diagnosed in a wide variety of experiments. These losses were originally described as an electron flow loss, which has since proven to be insufficient. Wire array calculations have typically utilized a post-dictive resistive convolute

loss, calculated on a shot by shot basis from the available electrical data. More recent particle in cell simulation work has indicated that this current loss likely results from the motion of cathode plasmas within the convolute [3]. Additional wire array work combining load calculations with electrical diagnostics has indicated the potential for additional current losses in close proximity to the arrays [4], although once again, the reliance on existing shot specific electrical data prevented this approach from being predictive. The development and magnitude of these current losses is strongly influenced by the voltage history of the imploding load, and yet significantly affects the load performance, so ideally must be self consistently accounted for. Furthermore, since they are localized, and driven by the current densities and voltages specific to their location, these losses must ideally be incorporated into a generator model capable of resolving these locations, rather than an extensively averaged or reduced circuit representation.

To begin to address these issues we couple an MHD model developed for compact tungsten loads, large diameter K-shell source loads and liners, to a transmission line representation of the Z generator. Extending previous work on transmission line driven MHD models of compact wire arrays, we rework the numerical solution scheme to reduce computational overhead and improve accuracy. This enables this model to be more broadly applied to a wider range of problems. Through comparison to the diverse and extensive data set amassed on Z, we describe a generic convolute current loss model, which we incorporate into a transmission line model and apply to different loads to study current delivery in these systems. Through comparison with electrical data we infer the need for additional current losses for some loads.

2. BACKGROUND

Existing work has been successful in parameterizing convolute current losses for application to compact tungsten wire arrays [4]. These specific loads are however no longer studied on Z, and losses of current at the convolute are understood to be somewhat load specific. It would be extremely useful to understand to what degree we can characterize the convolute loss, for application to other loads presently studied on Z, and to better understand how sensitive the load performance is to how current losses are captured.

2.1. Z architecture and Terminology

The work that follows primarily concerns the central section of the Z machine, out to a radius of approximately 2m. This region is shown in Figure 1 (a). It consists of four, cylindrically symmetric, magnetically insulated vacuum transmission lines (MITL's) [8]. Current is delivered to these lines, from a water section that is separated from the vacuum section by the insulator stack [14]. The four transmission lines are labeled A to D, from the top level to the bottom. The transmission lines are joined together by a double post hole convolute (Figure 1 (b)), that combines the transmission lines into a single power feed that connects through to the load region (Figure 1 (c)). As indicated in the figure the current and voltage are monitored on each of the four levels at the insulator stack. An additional current measurement is typically made by a b-dot placed behind one of the convolute anode posts on the A level at the top of the convolute [9]. This is indicated in Figure 1 (c), and is typically used to measure the total current exiting the convolute, and entering the final feed. While it is often referred to as the load current, for reasons that will become obvious later we will refer to it here as the convolute current. Load current will refer to the current that actually enters the load region at the end of the final power feed (or inner MITL feed). Ideally the convolute current and load current should be equal, but in this work we draw a distinction between the two by allowing for additional current losses to be located within the final feed. Given the location of the convolute current monitor we have no way of directly measuring any current loss within the final inner MITL feed.

Typical current measurements are shown in Figure 2 for the implosion of a nested wire array consisting of two cylindrical arrays of wires with an outer array diameter of 70mm [21]. This is the array depicted in the diagram of the final feed (Figure 1 (c)), and discussed in the following section. The current measurements show the total stack current summed over all four levels, compared to the convolute current measurement made at the exit to the convolute. The large difference between these two measurements is attributed to a loss of current within the convolute (referred to now as the convolute loss), and for some loads can account for several mega-amps of the total drive current.

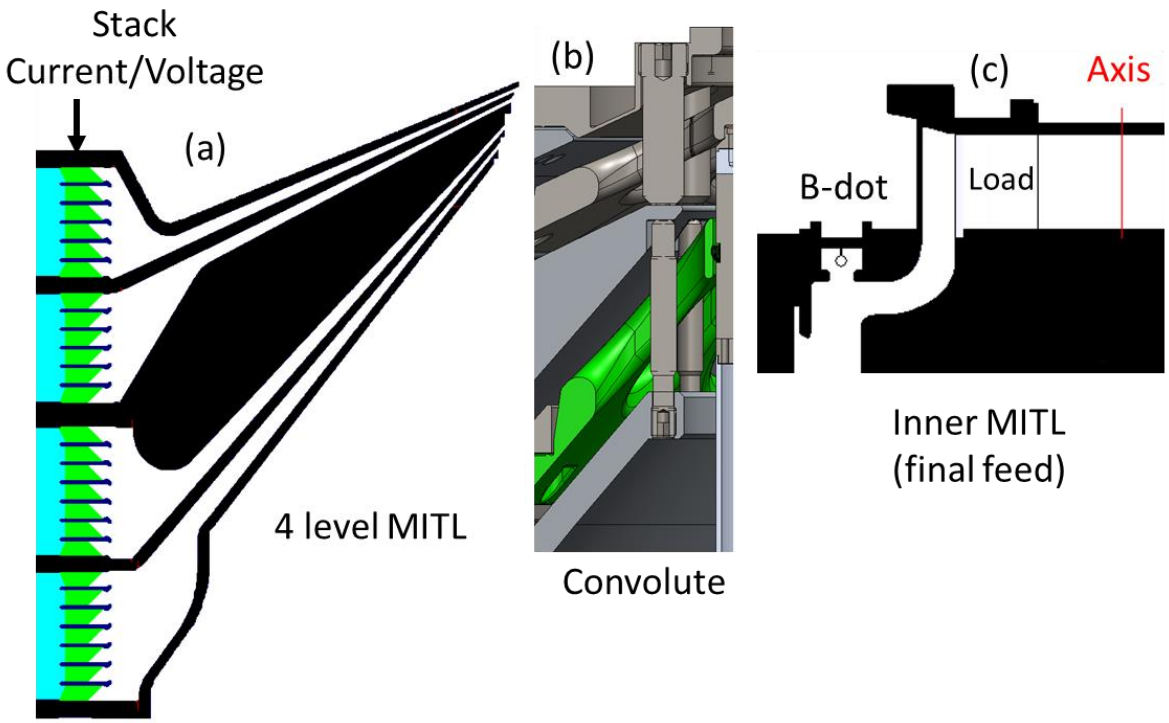

Figure 1. Central ~2m radius of the Z generator.

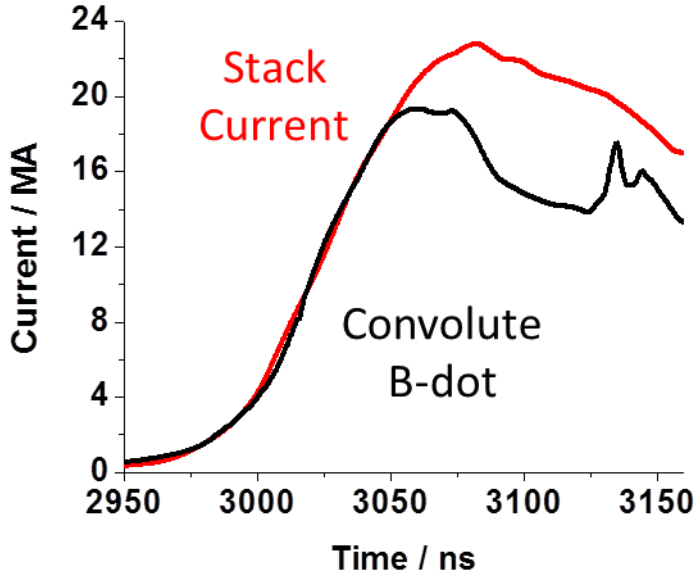

Figure 2. Stack and Convolute B-dot measurement for large diameter stainless steel load

2.2. Why details about the current delivery matter to the load

Taking as an example the loads on Z that operate as radiation sources [22], they work by applying a current to a cylindrically symmetric distribution of mass, and using the resulting jxB force to accelerate material towards the axis. As this plasma stagnates on axis, kinetic energy is thermalized and radiated. If we neglect the resistivity of the plasma, then as material is accelerated to smaller radius, the voltage over the load dramatically increases with the rapidly rising load inductance. When the voltage over the load gets high enough the current that can be delivered begins to drop in response. It is often stated that the array acts to temporally compress energy. We accelerate a plasma over ~100ns, building up its kinetic energy. We then stagnate the array, thermalizing and radiating that energy over just a few ns. With that understanding it is instructive to look at how energy is delivered to a typical imploding load. We use, as an example, a nested stainless steel wire array, consisting of two 20mm tall concentric arrays of wires, 70mm and 35mm in diameter. From simulations we can look at how energy is delivered to this array over the course of its implosion. Figure 3 shows the kinetic energy of the plasma compared to the load current delivered. As we can see, most of the kinetic energy is supplied in the very final stages of the implosion. For this array, 80% of the energy given to the plasma is delivered in the last 20% of the implosion. It is in these final stages that the current densities, magnetic fields, and velocities are highest, so the v.jxB work done on the plasma is also high. Furthermore, most of the kinetic energy is built up in the plasma after peak current as the voltage is rising and the current is dropping. When we are concerned with ensuring a simulation accurately determines the energy delivered to the load to be radiated, it is not enough to simply get the correct peak current, and assume late time energy delivery is unimportant. It is the approach to stagnation, when the current is falling, that most energy is delivered to the plasma. It is also during this time, while the voltage is rising, that any current losses will be at their worst. To be confident we are delivering the correct energy to the load we must accurately reproduce the current profiles, not just around peak current, but throughout their fall from peak. And while the details of current losses can affect the peak current reached, they can have a more dramatic effect in determining the rate at which the current falls.

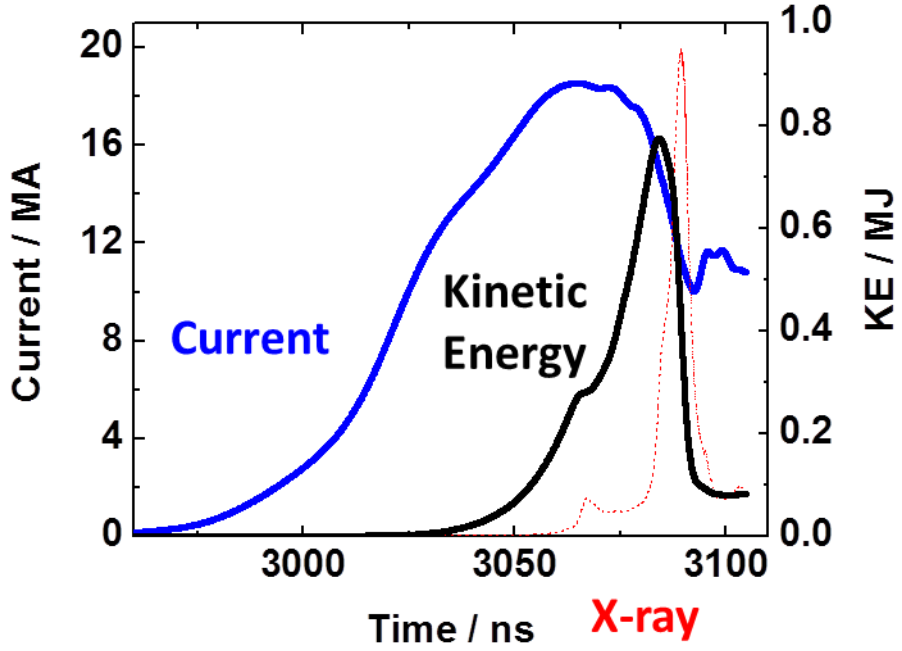

Figure 3. Current and Kinetic Energy for Large Diameter Stainless Steel Wire Array

2.3. Present understanding of the causes of convolute loss

Particle in cell calculations of the convolute region performed by D. Rose [3] have indicated that significant current loss can occur when plasma sourced from the cathode moves around the convolute and bridges the gap between the cathode and the anode post on the load side. Experimental work by M. Gomez [24] has confirmed the motion of plasma within the convolute. Previous work to drive compact tungsten loads with a circuit model that accounted for the loss of electron flow current at the convolute has demonstrated that this loss mechanism is insufficient to explain the magnitude of current loss observed for loads on Z. The work had to invoke an additional short circuit component to drive the observed current loss, which is certainly consistent with plasma moving across the convolute as demonstrated by the Rose calculations. For much of this work, electron flow contribution to the current loss is therefore neglected, in favor of a resistive short circuit forming at late time.

3. REPRESENTING THE Z GENERATOR

A prerequisite to studying the coupling between an MHD model of an imploding load, and the Z generator is appropriately characterizing the circuit behavior of the Z generator. For the purposes of this work we would like to capture the response of the generator to the rising inductance of the load, whilst retaining a model simple enough to run in-line with our load calculations. The principle, diagnosed problem in delivering current to the load region is the loss of current at the convolute, so our model must retain sufficient complexity to accurately represent the voltages and currents at the location where this loss occurs.
For these reasons we will limit ourselves to a radius from the load that encompasses the vacuum section, the water/vacuum insulator stack, and the start of the water lines that connect to the insulator stack. The generator architecture beyond this radius is extremely complex, and has already been modeled in detail [1]. However, for our purposes, many of these details are essentially transit time isolated from the most violent stages of implosion and stagnation. We therefore represent the bulk of the generator as an ideal voltage source we apply at the water section joining the insulator stack, and focus our attention on representing current delivery through the vacuum section. Future work can attempt to assess how much of the generator should be modeled in-line with load calculations. Such work would however require accurately capturing current delivery through the vacuum section as a starting point.

For reasons that will be discussed in more detail later the circuit representation we choose must be compatible with the electromagnetic field solution scheme used in the resistive MHD code we will use to model the load. For this reason we use a series of lumped circuit element transmission lines to represent the insulator stack and vacuum transmission lines. The convolute is represented by a series of inductors coupling these lines. The final feed section that joins the convolute and load is either represented by another lumped circuit element transmission line, or by a simple inductor. The capacitance and inductance profiles forming these transmission lines are calculated either directly from the hardware geometry, or from electromagnetic simulations of a section of the transmission line.

3.1. Vacuum Lines

The capacitance and inductance profiles of the four vacuum transmission lines that connect to the convolute are calculated directly from the transmission line geometry, which is taken directly from the technical drawings. The anode and cathode profiles we represent are displayed in Figure 4 (a). For simplicity we construct inductance and capacitance profiles as a function of radius, rather than length along the line. At a given point the inductance (L) of an element of width dr=1.e-3 is calculated according to the integral of the magnetic energy contained in that element:

$$L = h \int_{r-dr/2}^{r+dr/2} \frac{\mu_0}{2\pi r} dr$$

Where h is the vertical distance between anode and cathode. The corresponding capacitance (C) of this element is then calculated according to:

$$\tau = \sqrt{\frac{LC}{dr^2}}$$

Where τ is the transit time across the element of width dr. This assumes speed of light propagation along a path length dl, which is the average of the length of the anode and cathode surfaces across the width dr. Since the 4 transmission lines approach the load at different angles, this ensures we capture the different propagation times down each line. The resulting capacitance and inductance profiles for this vacuum section are shown in Figure 5, with the profiles through the insulator stack included, and discussed in the next section. We have followed the lines down to a radius of 11.6 cm, which for this work is the point we define to be the start of the convolute. Working from the transmission line geometry in this way it is a simple matter to allow for changes in the line profiles from the expansion of electrode plasmas.

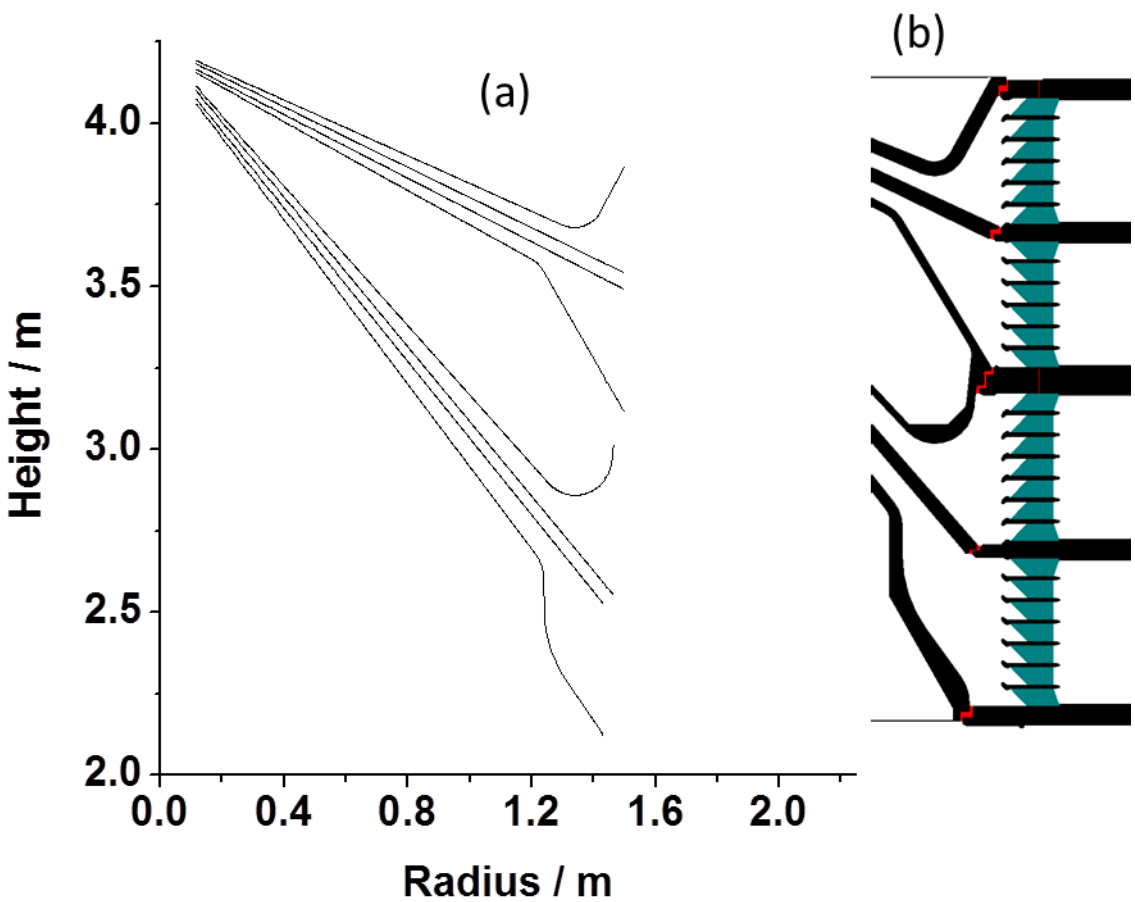

Figure 4. Scaled Profiles of the MITL's, and diagram of the insulator stack

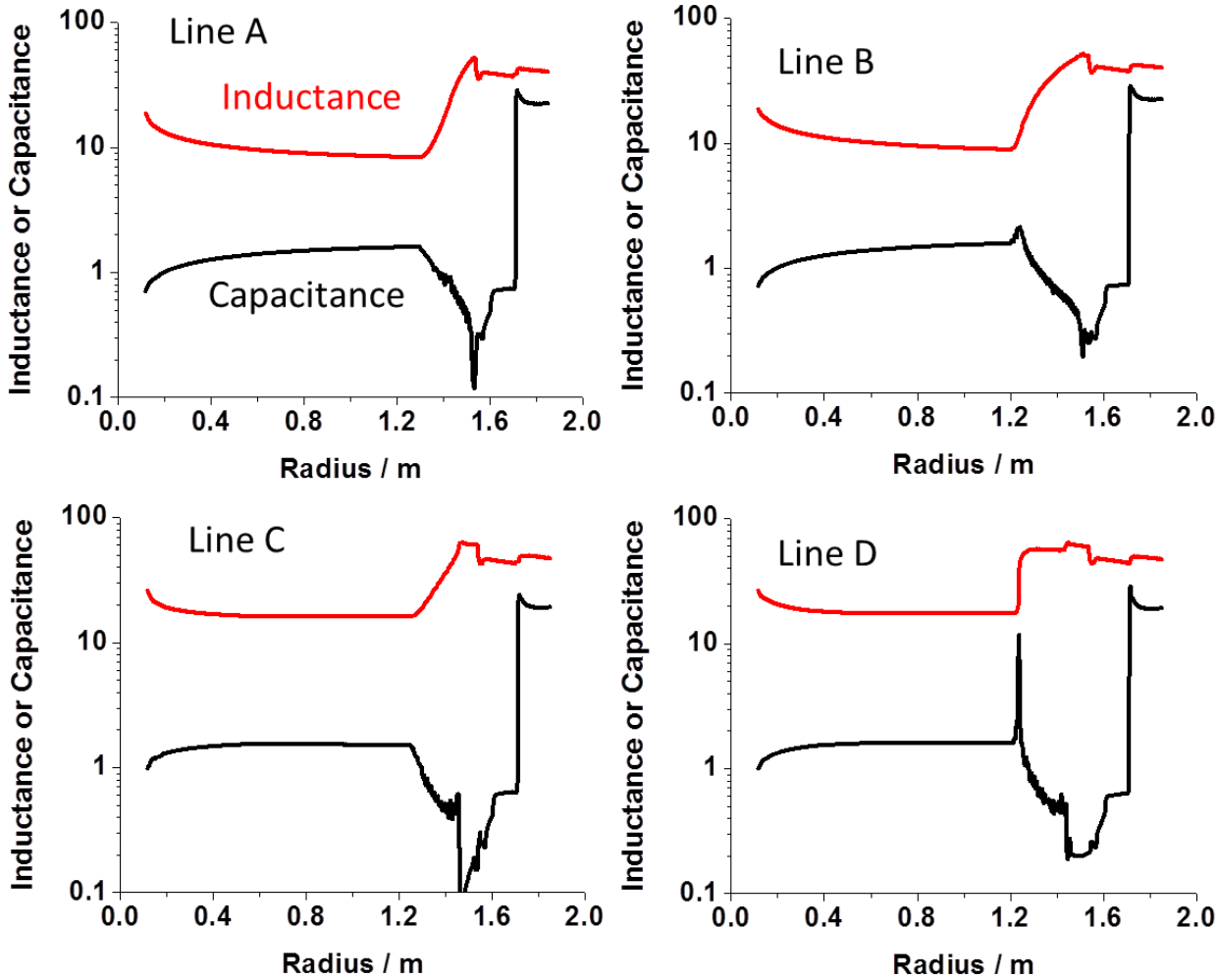

Figure 5. Capacitance and inductance per unit length. nF/m and nH/m

3.2. Insulator Stack

The interface between the water and vacuum sections consists of a series of rexolite rings separated by metal Figure 4 (b) Given the complicated geometry a transmission line equivalent of this section is formed by performing an electromagnetic simulation of a region extending from a radius of 1.2m, through the stack to a radius of 1.85m. For the 4 transmission lines of Z this encompasses the insulator stack and the start of the water lines, as shown in Figure 4(b). It also provides some overlap with the vacuum line sections previously calculated, to ensure we can correctly join these sections into a continuous line.

The calculation is performed using the same resistive MHD code later used to model the load region, which has been built around an electromagnetic field solver. Metal sections forming the line are assumed to have a constant resistivity of 6.9e-7 ohm-m. Changes in the permittivity are affected by appropriately modifying the speed of light to assign a relative permittivity of 1 in the

vacuum region, 2.53 for the rexolite insulator rings, and 80.1 for the water. The calculation is performed by shorting out the load end of the transmission line and setting a varying current at the start of each line. At each radial location we integrate the electric field in z across the line to determine voltage, whilst averaging the total anode and cathode currents at that radius to determine total current. We then calculate equivalent inductances and capacitances according to the telegrapher's equations:

$$\frac{L}{dr} = \frac{-\frac{\partial V}{\partial r}}{\frac{\partial I}{\partial t}} \qquad \frac{C}{dr} = \frac{-\frac{\partial I}{\partial r}}{\frac{\partial V}{\partial t}}$$

Since changes in the voltage and currents over a given radial element can be small the current applied is varied sinusoidally with a period of 200ns and magnitude of 20MA, so that inductance can be determined at peak dI/dt, and capacitance determined at peak dV/dt. The resulting capacitance and inductance profiles across the insulator stack are shown in Figure 5. The stack current and voltage probes are located within the stack, so when we later make use of these measurements we require a transmission line that passes through it. These simultaneous current and voltage measurements are used extensively to determine the current and voltage at the convolute, and to construct equivalent voltage sources with which to drive the calculations we later discuss. The way in which we construct a voltage source to drive this system is described in [4].

4. CHARACTERIZATION OF THE CONVOLUTE LOSS

The principle, diagnosed, problem with electrical power delivery to the load region is a loss of current at the convolute. An equivalent circuit to drive load calculations must adequately represent this loss. To measure this loss a b-dot is typically located just inside the convolute to determine the current delivered to the load. Current delivered to, and the voltage at the convolute are not directly measured, but may be reconstructed from the simultaneous current and voltage measurements made at the insulator stack. From knowledge of the current lost, and the voltage at the convolute we can construct a time dependent resistor to ground.

Procedures for accomplishing this have previously been developed for compact tungsten wire arrays [4], and are applied here to a number of different loads to determine how convolute losses may vary between different experiments. A variety of different load configurations have been fielded on Z, enabling us to examine convolute losses for a number of different initial load inductances, implosion times and voltage time histories.

One concern with the previous approach [28] has been azimuthal variation in the current and voltage at the stack, and the affect this may have on the translation of these measurements to the convolute. To assess this for a typical load we make a modification to the routines previously used to translate the voltage and current measured at the stack down to the convolute region. For each of the 4 transmission lines there are approximately 16 voltage and current probes azimuthally spaced around the insulator stack. For a given shot there is typically some azimuthal variation to the electrical power delivered to the stack (Figure 6). While this does homogenize as we approach the convolute, it is not technically correct to simply average the measured currents and voltages and then translate them. The translated average measurements are not necessarily equal to the average of the translated measurements.

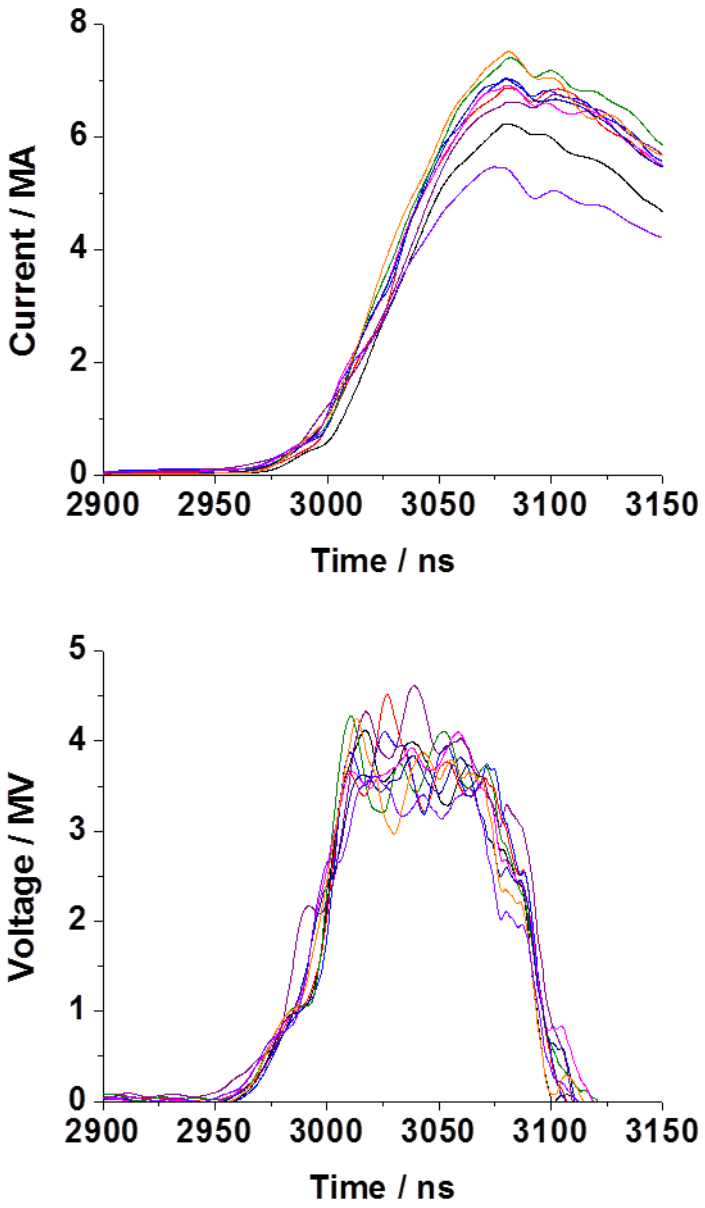

Figure 6. Multiple current and voltage measurements at different azimuthal locations in the stack (Z shot 2235)

To examine the effect of this we take the currents and voltages at different azimuthal locations and linearly interpolate between adjacent measurements. With this we calculate the current and voltage over each of 9 separate transmission line sections equally spaced azimuthally. These 9 sets of currents and voltages are then separately translated down to the convolute, before being averaged to construct the convolute voltage and current. Since we do not allow propagation between adjacent sections this does represent a worst case scenario of azimuthal variation reaching the convolute. If however there is strong azimuthal variation at the stack it does

prevent the error incurred when voltage from one side can essentially see the current from the other and create a fictitious wave structure to propagate down the transmission lines. This approach also results in an algorithm that may later be modified to account for azimuthal propagation of signals. Applying this translation approach to stainless steel 70mm diameter load data (Z shot 2235) we compare the resulting voltages at the convolute for the A level, with those previously obtained by averaging the stack measurements before translation (Figure 7). We see negligible difference between these measurements, giving us some confidence that this effect is small for these types of loads.

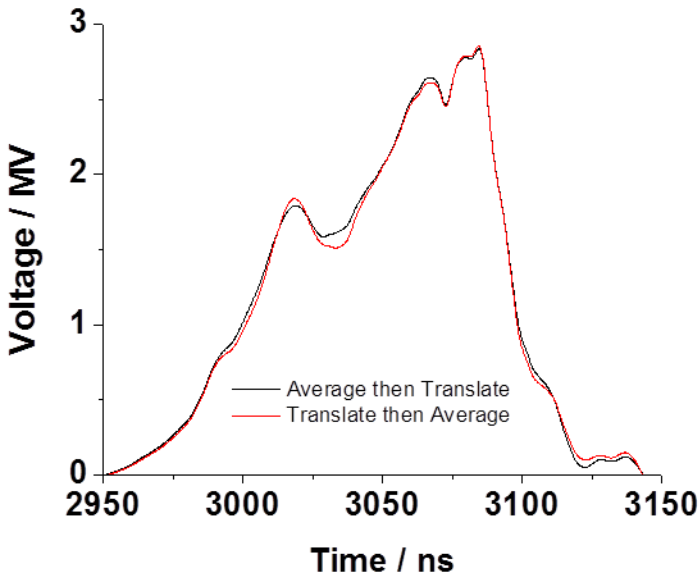

Figure 7. Average translated voltage compared to translated average voltage for the A level

4.1. The Measured Convolute Loss on Z Experiments

For application to a circuit model we ideally require a generic, time dependent resistor that can represent the convolute behavior for a wide variety of loads. To assess the variability of the convolute loss resistance we first calculate it for a number of different experiments, spanning different initial load inductances, and voltage time histories. For our purposes the initial inductance we quote is the total inductance downstream from the entrance to the convolute (radius of 11.6cm) on the top transmission line (the A level). This includes the inductance of the top of the convolute, the power feed connecting to the load, and the initial load inductance. The entrance to the convolute is also the location we translated stack voltage and current measurements to, which we use to construct the time dependent resistances shown. Specifically, the current into the convolute is the sum of the translated stack currents from all 4 transmission lines. The current out of the convolute is measured by a b-dot which is typically inside the convolute anode posts. The voltage at the convolute is just the translated stack voltage on the A

level. For clarity these measurement locations are indicated in Figure 8. Convolute voltages may also be calculated from the other transmission lines, but these measurements see the load through additional convolute inductances which are different for each line, and can be difficult to quantify. For many load configurations repeat shots have been made, enabling us to also understand how reproducible the convolute behavior is for a fixed configuration. Many of the loads imploded on Z are high power x-ray sources, so where relevant the convolute resistances are plotted with a normalized x-ray pulse shape to indicate the time at which the load imploded on axis. We now calculate convolute losses for a number of different loads. For each load we show the convolute resistance, and the current and voltage measurements from which it was calculated.

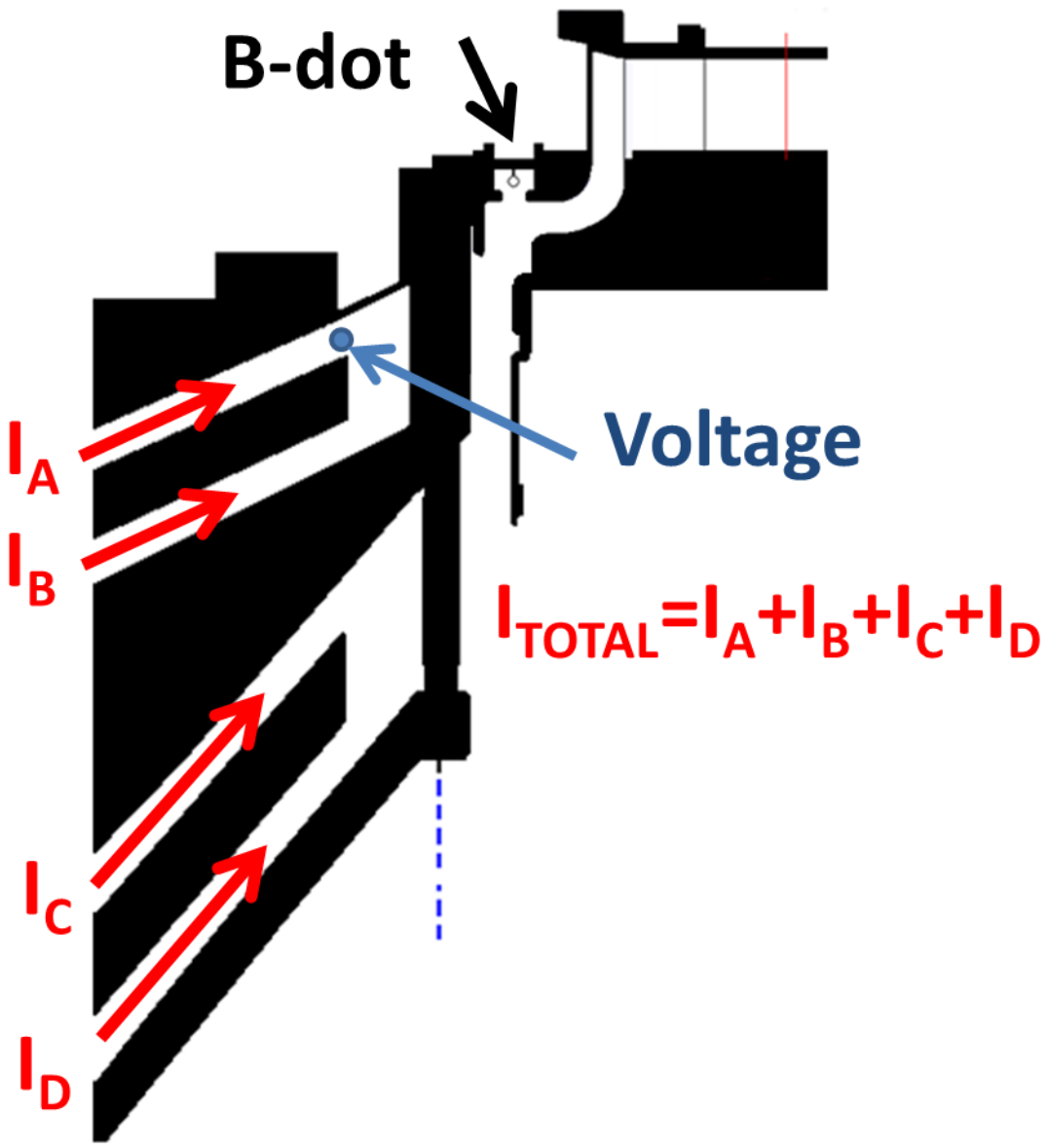

Figure 8. Convolute current and voltage measurement locations

4.1.1. Large diameter (70mm), low mass stainless steel arrays.

These experiments were fielded by David Ampleford [22,29]. These loads are used to study the generation of K-shell radiation at high photon energies, which for materials like iron necessitates very high temperatures during stagnation. These high temperatures are achieved through the rapid thermalization of implosion kinetic energy, requiring the average kinetic energy per ion to exceed the photon energy being studied by typically at least a factor of 2. As such, very large implosion velocities are required for higher Z elements.

These experiments used nested wire arrays that are 2cm in height, with a 2:1 mass ratio between the outer and inner wire arrays. For these loads (Z shots 2234-2237) 112 wire outer arrays imploded on 56 wire inner arrays with a total load mass of 1.5mg. The diameter of the inner array was half that of the outer array.

These large diameter arrays typically have a very low initial inductance (5nH) due to the large initial diameter. They are however very low mass, set to implode before peak current. Since the load design is intended to reach very high velocities they generate very large voltages from their rapidly changing inductance. They also converge to very small diameters (~0.9mm) resulting in a very large final inductance. As such, while the initial voltage developed over the convolute is quite low, the final voltage is the highest of the experiments we study here. From Figure 10 we see that the convolute resistance collapses to a value of ~0.7ohms ~17ns before stagnation. Following the x-ray power pulse the resistance is seen to further decay.

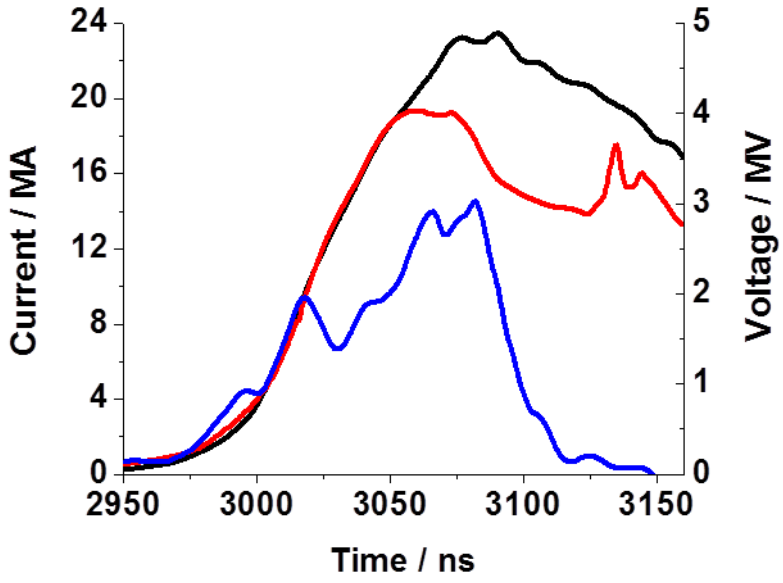

Figure 9. Translated Stack Current / Convolute Current and Convolute Voltage

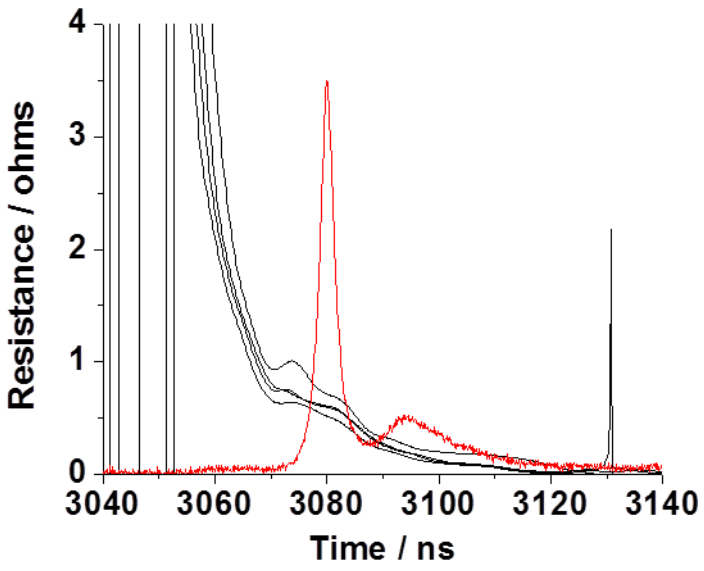

Figure 10. Convolute resistance with normalized total x-ray power pulse

4.1.2. Higher mass 65mm diameter stainless steel arrays..

These experiments were fielded by Brent Jones [24] and Dave Ampleford [22]. While similar in many respects to the 70mm diameter low mass arrays, these experiments were at a smaller initial diameter, and used more mass, to implode later in the current pulse. These experiments used nested wire arrays that are 2cm in height, with a 2:1 mass ratio between the outer and inner wire arrays. For these loads (Z shots 1857 and 1860) 200 wire outer arrays imploded on 100 wire inner arrays with a total load mass of 2.48mg. The diameter of the inner array was again half that of the outer array. Due to the smaller diameter array, and changes in the anode/cathode gap spacing approaching the array, the initial inductance of this load was higher (~6nH). While this generates a higher voltage over the convolute initially, the longer implosion time, and smaller final implosion velocity leads to a lower voltage at stagnation. From Figure 12 the convolute resistance is seen to collapse to a value of ~0.65 ohms at around ~35ns prior to stagnation. The resistance remains approximately constant until stagnation, before decaying a few ns after peak x-ray power.

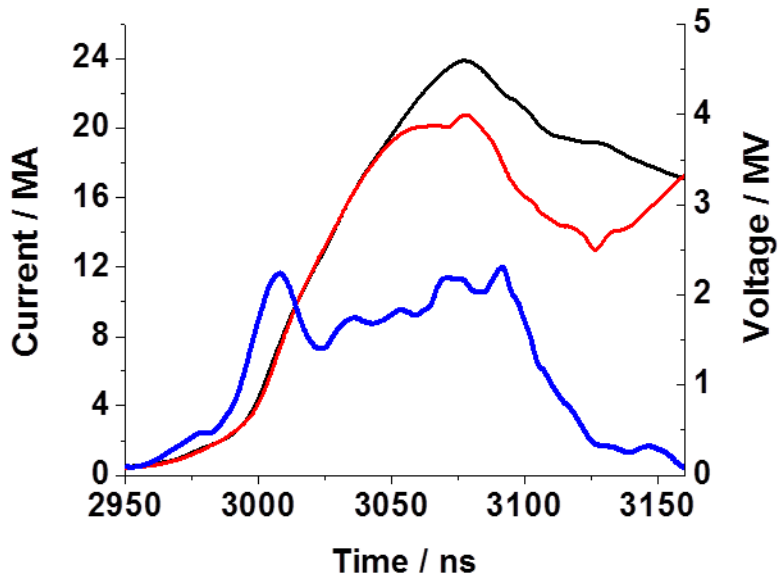

Figure 11. Translated Stack Current / Convolute Current and Convolute Voltage

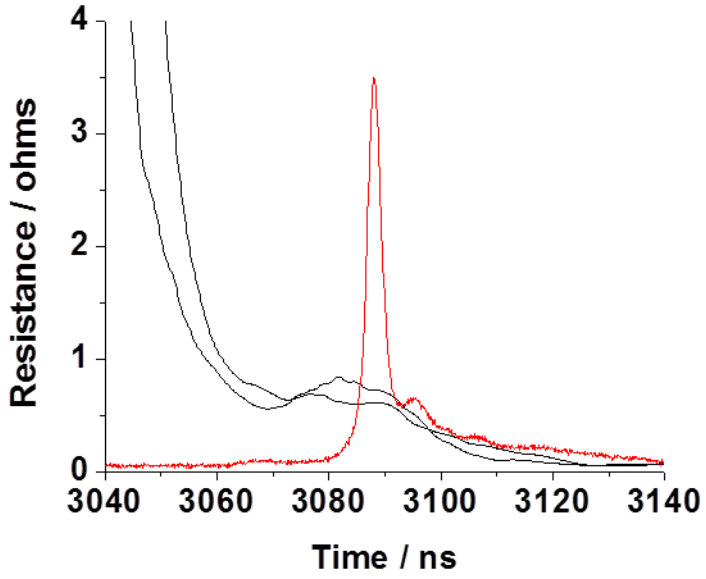

Figure 12. Convolute resistance with normalized total x-ray power pulse

4.1.3. 65mm Nested tungsten wire arrays.

These experiments were fielded by Michael Jones [27]. These loads (Z shots 1994-1999) used essentially the same setup and load mass (~2.5mg) as the 65mm stainless steel arrays. They were conducted by the Z facility to investigate high power x-ray sources and address machine development needs. From Figure 11 we can see that the current delivery and convolute resistance are very similar to the results obtained with the stainless steel arrays. The convolute resistance collapses to a value of ~0.69 ohms before remaining constant and then further decaying after the x-ray pulse.

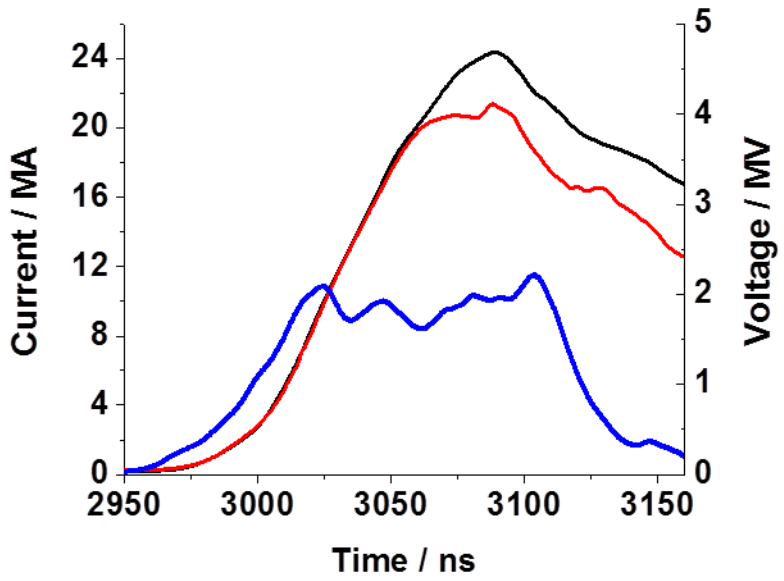

Figure 13. Translated Stack Current / Convolute Current and Convolute Voltage

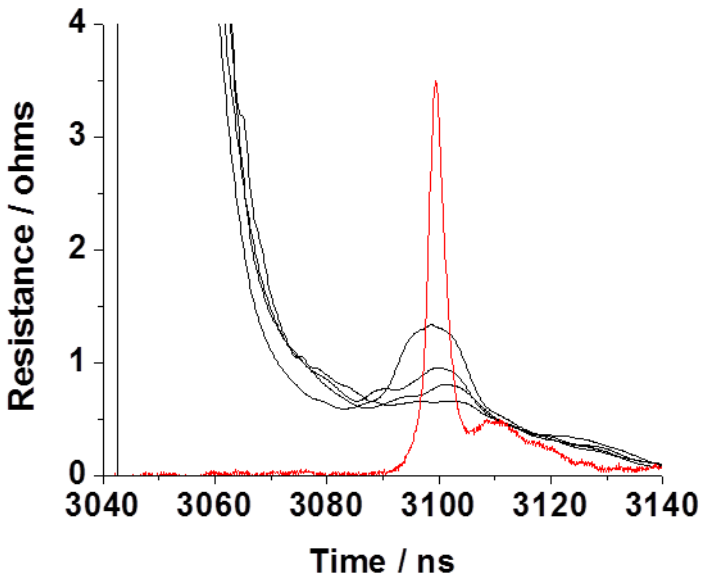

Figure 14. Convolute resistance with normalized total x-ray power pulse

4.1.4. 65mm Nested Copper wire arrays.

These experiments were fielded by Brent Jones [25]. Again, repeating the initial array setup of the 65mm stainless steel and tungsten array shots, these loads (Z shots 1975 and 1977) used approximately the same mass (2.58mg), although with a lower wire number (96 on 48). Due to changes in the design of the power feed connecting convolute and load, these shots also had a smaller initial inductance (5nH). From Figure 16 the convolute resistance is seem to collapse to ~0.65 ohms, where it remains constant before further decaying after stagnation, essentially repeating the behavior of the other 65mm loads. The time at which the convolute resistance collapses does however appear to be ~7 ns later than the previous results. While the final convolute resistance does appear consistent with the other 65mm loads, this does potentially indicate that higher initial inductances may lead to an earlier "turn on" of the convolute current loss. This shot series also included a heavier copper array (shot 1976) which used the same shot configuration, but had a total mass of 3mg (112 wires on 56). Figure 17 compares the convolute loss resistance for these two different massed loads, demonstrating the same initial collapse to constant resistance. The post stagnation decay is however later in the heavier shot, corresponding to the later implosion time. This demonstrates the final decay of the convolute resistance correlates well with the x-ray pulse generated at stagnation.

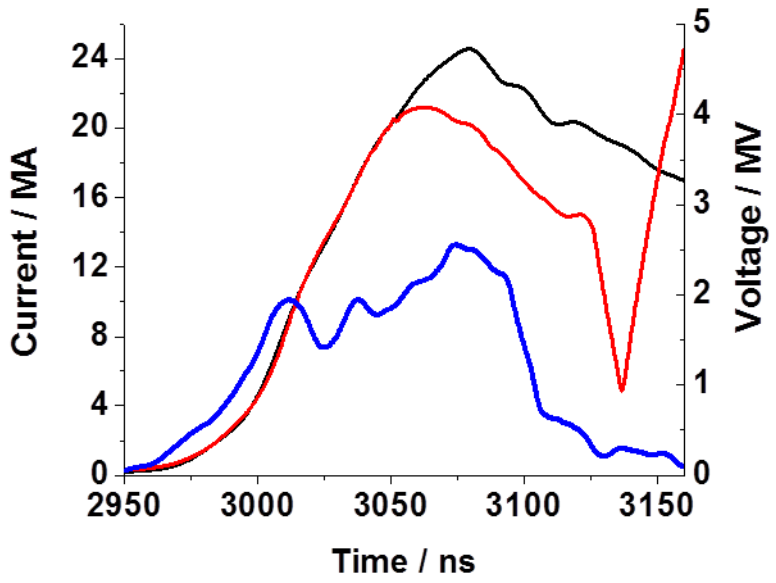

Figure 15. Translated Stack Current / Convolute Current and Convolute Voltage

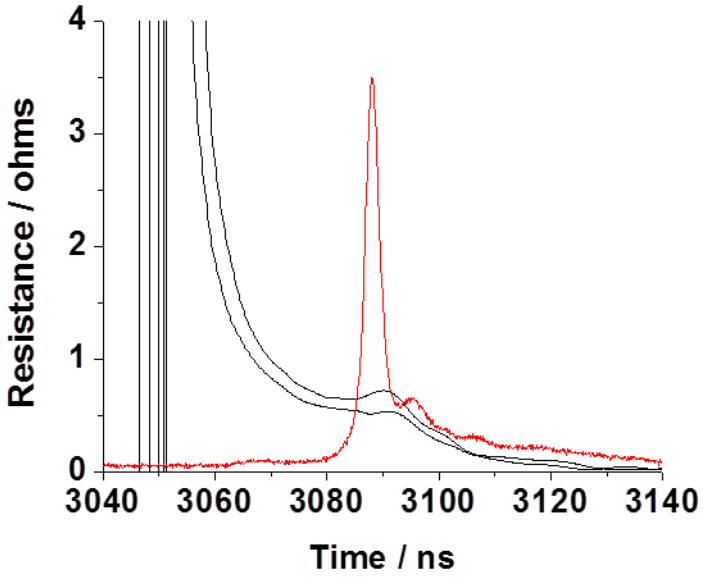

Figure 16. Convolute resistance with normalized total x-ray power pulse

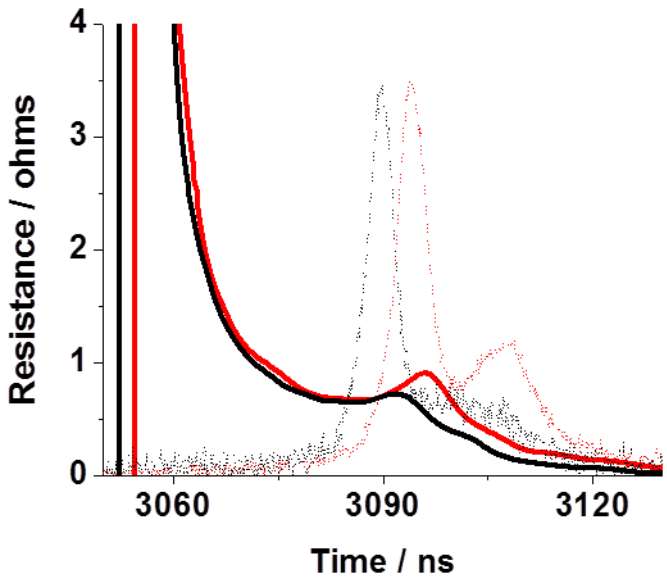

Figure 17. Convolute resistance with normalized total x-ray power pulses for two different array masses

4.1.5. Large diameter (50mm), low mass Aluminum arrays.

These experiments were fielded by David Ampleford [23]. These are nested wire arrays that are 2cm in height, with a 2:1 mass ratio between the outer and inner wire arrays. For these experiments (Z shots 2334-2338) 176 wire outer arrays imploded on 88 wire inner arrays with a total load mass of 2.13mg. Like the 70mm diameter stainless steel arrays these have relatively low mass, low initial inductance (5.2nH), and implode at high velocity to generate large final voltages. However, the lower radiation loss rate of Aluminum, compared to Stainless Steel, results in a larger final pinch diameter and a much broader x-ray pulse. From Figure 19 we again see the convolute resistance collapse before peak x-ray power, however it now continues to decay. Previous results indicate the convolute resistance drops to a fixed value, remains constant, and then continues to decay after the start of the x-ray pulse. These separate stages may not however be distinguishable in this case. From previous results it seems plausible that radiation from the stagnation is initiating the late time decay of the convolute resistance. However in this case there is little separation between the convolute resistance collapse, and a stagnation that results in a very broad x-ray pulse. It is possible that radiation from these loads may be initiating the late time decay of the convolute resistance sooner. What we see as a continued decay of the convolute resistance may potentially be an artifact of the close proximity of stagnation to the onset of current loss. Since, for this implosion, the convolute resistance is able to decay significantly over the duration of the x-ray pulse, we might be able to better maintain current delivery by better screening the convolute from load radiation. However, this would probably only benefit loads that resulted in very broad x-ray power pulses.

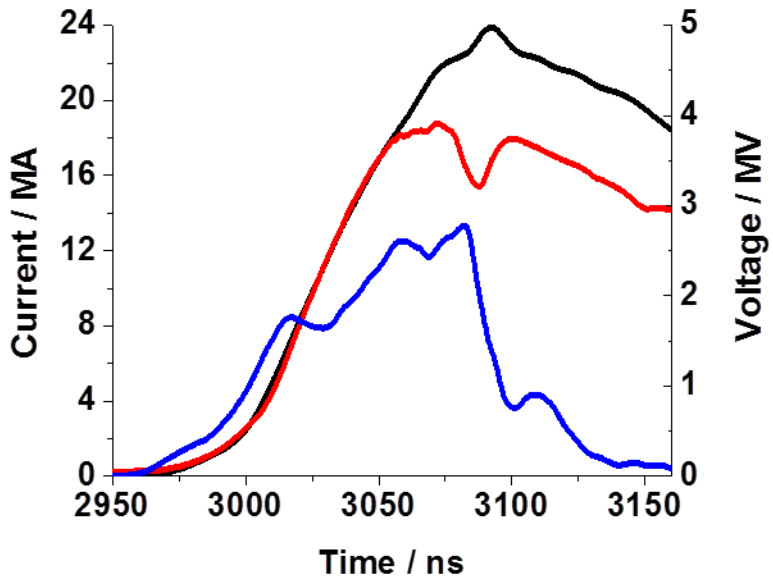

Figure 18. Translated Stack Current / Convolute Current and Convolute Voltage

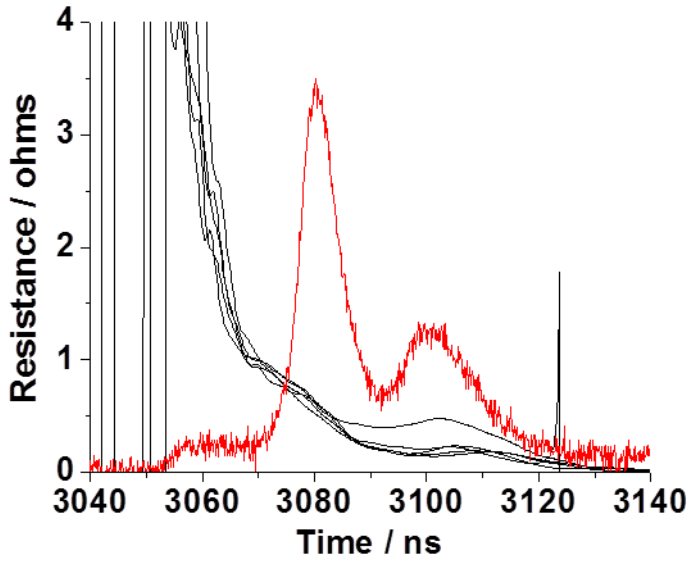

Figure 19. Convolute resistance with normalized total x-ray power pulse

4.1.6. Dynamic Hohraums.

These experiments were fielded by James Bailey [15]. These experiments used nested wire arrays that are 1.2cm in height, with a 2:1 mass ratio between the outer and inner wire arrays.

For these loads (Z shots 2299-2302 and 2363-2367) 240 wire, 40mm diameter outer arrays are imploded on 120 wire, 20mm diameter inner arrays with a total load mass of 8.16mg. While having a smaller initial radius they are only 12mm tall, so they have the lowest initial inductance (4.9nH) of the loads we study here. They have extremely high mass, imploding well after peak current, and stagnate upon a massive cylindrical foam target (6mm diameter, 14.5mg/cc) placed on axis. The stagnation of the array onto the foam target creates a very uniform radiation source which is then used to drive additional experiments. Given the high mass, and long implosion time, these loads have a relatively low implosion velocity, so the voltage they put over the convolute remains comparatively low. As shown in Figure 21, the convolute resistance is seen to collapse to around 0.75 - 0.79 ohms, where it remains roughly constant until stagnation, after which it decays. Compared to the previous loads we've looked at more variability is seen in these convolute resistances. These resistances are significantly more sensitive to small errors in the b-dot measurements. If convolute resistances are consistent between different loads, then the low voltages developed by dynamic hohlraum loads will drive a much smaller convolute loss. In calculating the resistances we are therefore dividing by a small number (the current loss). When the current loss is large (as in the previous light, large diameter loads), a few % error in the load b-dot measurement has little effect on the current loss calculated. When the convolute loss is low, any small variation in the load b-dot measurement will have a much bigger effect. Despite this, the convolute resistances are generally consistent, indicating the same collapse to constant impedance that is seen in other loads.

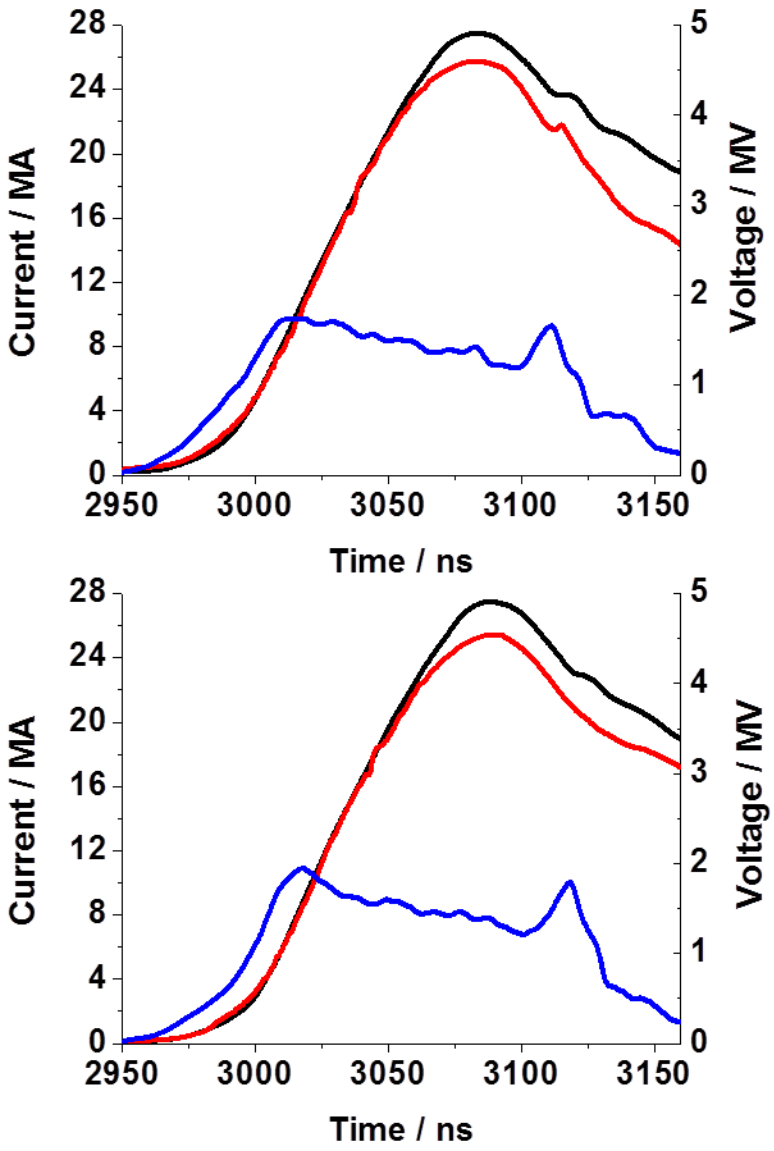

Figure 20. Translated Stack Current / Convolute Current and Convolute Voltage

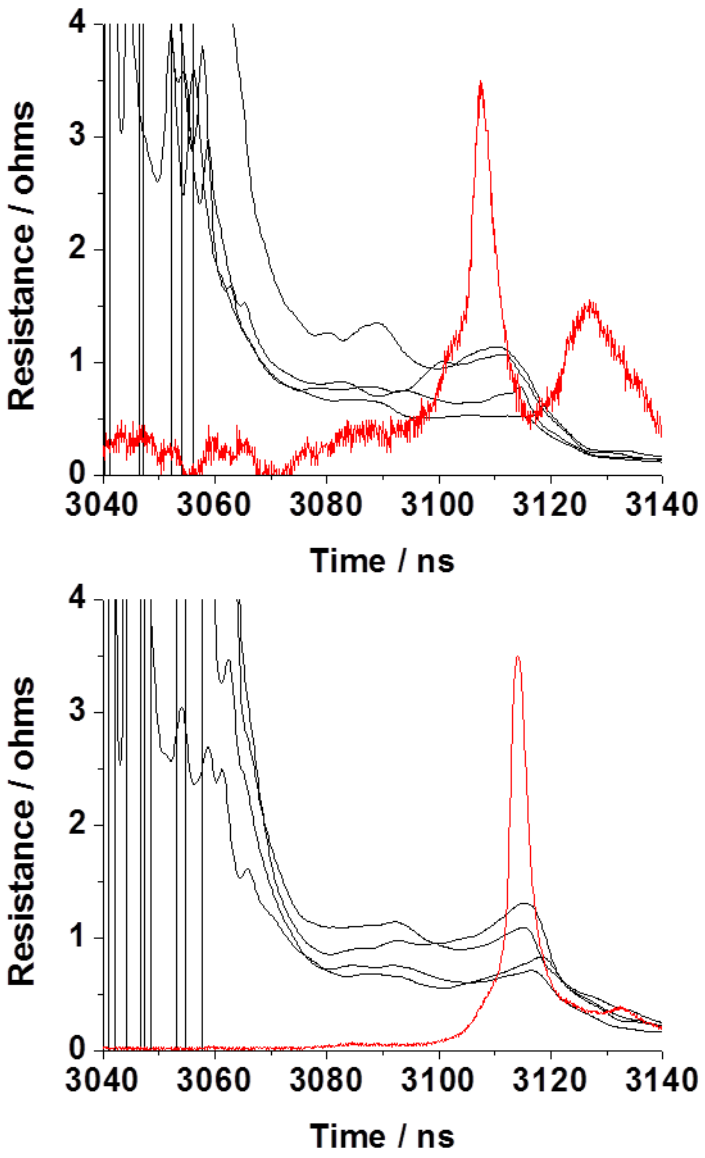

Figure 21. Convolute resistance with normalized total x-ray power pulse

4.1.7. MagLif style liners

These experiments were fielded by Ryan McBride [19,20]. The MagLif fusion scheme [21] recently proposed requires the implosion of a small cylindrical liner, which is hoped will compresses a preheated deuterium/tritium gas to fusion temperatures and densities. In support of this concept a number of cylindrical beryllium liners have been imploded on Z. The liners we look at here are 6.5mm tall, and have inner and outer radii of 2.89mm and 3.47mm [19] respectively.

These targets are also high in mass, so implode well after peak current. They start from small radius, and so have a high initial inductance (7.2nH). More recently they have been fielded with a longer, raised power feed to accommodate magnetic field coils intended to magnetize the load and suppress thermal conduction. This has further increased the initial inductance (by ~0.8nH), and appears to have reduced the current delivered [20]. Since they are massive, and implode slowly they develop little voltage during implosion, but they do start and end at a very high fixed inductance. Figure 21 and Figure 23 shows that the convolute loss resistances for the standard, and raised loads behaves quite differently to the previous wire array results. The resistance is seen to continuously decay to a much smaller value. It is the voltage over the convolute that typically drives the current losses through it, so these small convolute resistances are attributable to the current losses occurring at a time when the convolute voltage has dropped to a very low value.

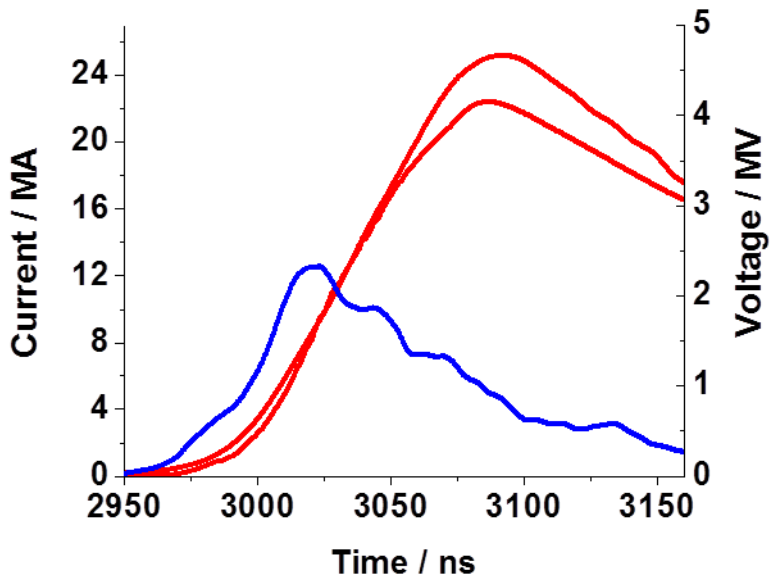

Figure 22. Translated Stack Current / Convolute Current and Convolute Voltage for Z2105

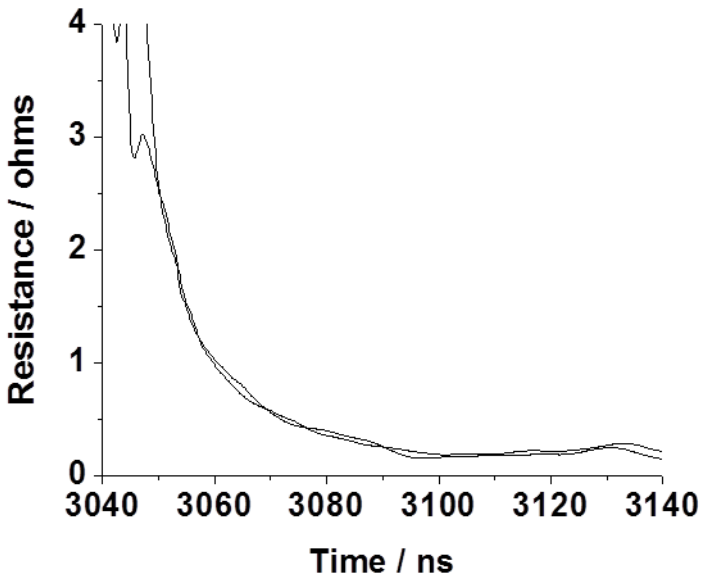

Figure 23. Convolute resistance Z2105

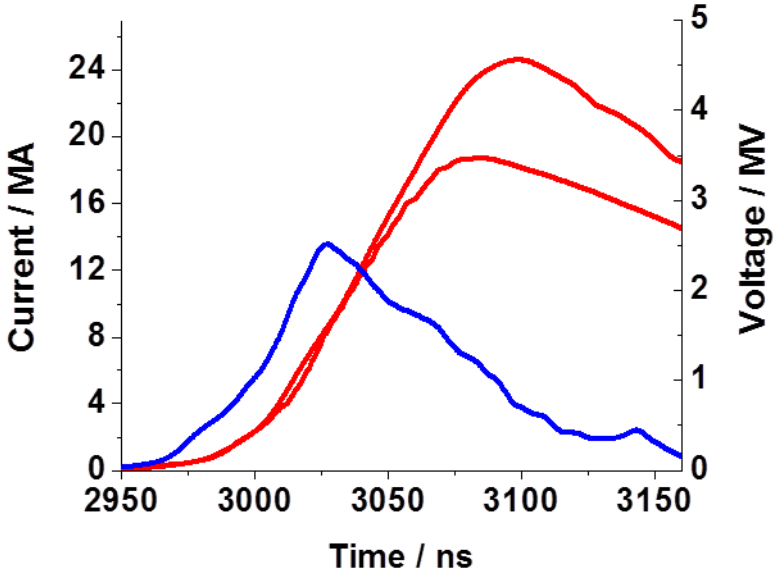

Figure 24. Translated Stack Current / Convolute Current and Convolute Voltage for raised feed

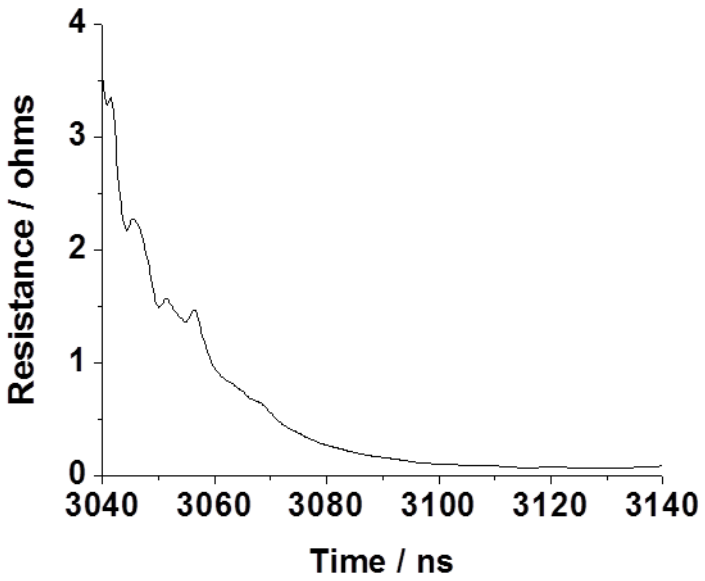

Figure 25. Convolute resistance for raised feed

4.1.8. 8cm diameter Krypton gas puff

This shot was fielded by David Ampleford. These gas puff loads are the largest loads that can be fielded on the existing convolute. They are low mass, imploding at very high velocity, developing a large voltage from a rapidly changing inductance. There is essentially no separation between the load and the entrance to the convolute. Multiple b-dots were fielded at different locations for this experiment, and large variation between the different measurements lead to very large uncertainties in assessing the convolute resistance for this shot. In a manner that will be discussed in more detail in section 5, using MHD simulations of the load implosion we determine a drive current that is consistent with the voltage measurements. From this guidance, the convolute resistance we calculate here uses the b-dot measurement that most closely follows the load current inferred from the stack voltage. This results in the convolute resistance behavior shown in Figure 27. The convolute resistance collapses early and continues to decay to a low value. In general the current delivery to this load appears to be poor, due to an extremely large convolute loss. Although given potentially large uncertainties in deciding which b-dot was most representative of the load current, this convolute resistance may not be representative of the convolute behavior. Hopefully future experiments may allow these conclusions to be refined.

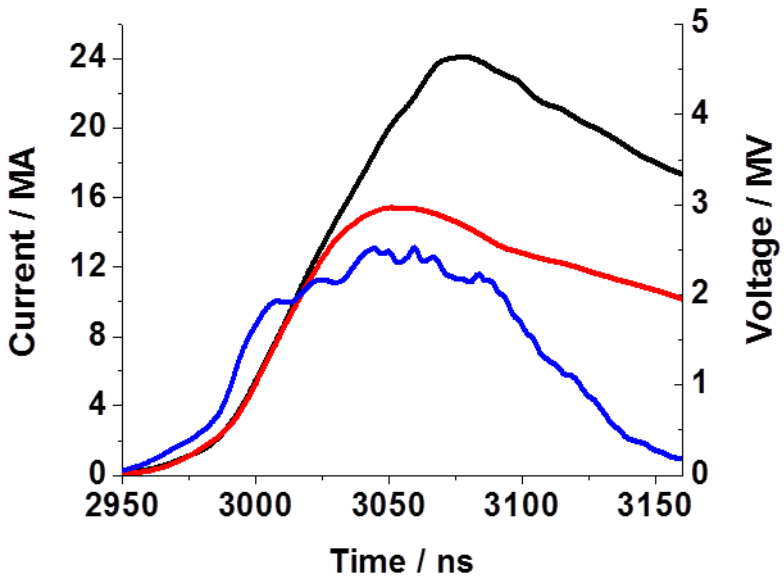

Figure 26. Translated Stack Current / Convolute Current and Convolute Voltage for Kr gas puff

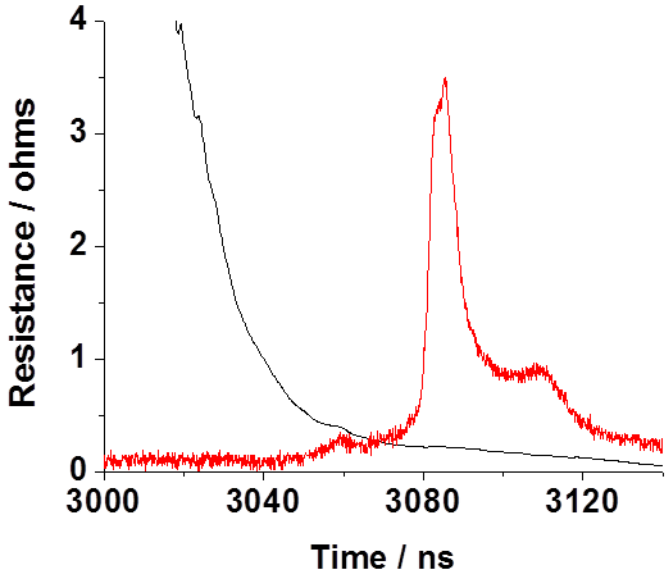

Figure 27. Convolute resistance and normalized total power for Kr gas puff

4.2. Constructing a Generic Convolute Loss

With the exception of the convolute loss resistance calculated for the MagLif liner implosions, and the Kr gas puff, the resistance behavior of the convolute appears to be remarkably consistent. At a point in the current rise the convolute resistance is seen to drop to a value of ~0.75 ohms, where it remains approximately constant until the load stagnates, after which it decays further. Representative resistances from the variety of different loads we've looked at are shown in Figure 28. For reasons that will be discussed in more detail later, the MagLif liners and gas puff are not included in this comparison. While the resistance behavior is consistent, there does seem to be some variation in the time at which the current loss begins. For the shots we've examined Figure 29 plots the current loss start time against initial load inductance. For this comparison, the time at which the convolute resistance collapses is defined as the time between the stack current reaching 7.48MA, and the convolute resistance dropping below 2 ohms. Over the range of initial inductances we've examined the resistance collapse time seems to be consistently ~50ns, with a trend towards higher initial inductances resulting in an earlier resistance collapse time. Figure 30 shows the range of load voltages which correspond to the convolute resistances calculated, showing that this behavior appears to remain consistent over a broad range of voltages.

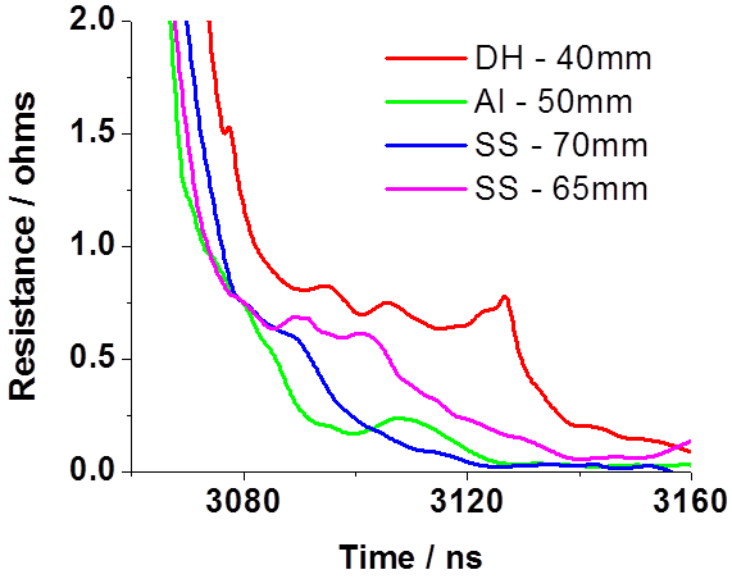

Figure 28. Convolute resistances for dynamic hohraum, 70mm stainless, 50mm Aluminium and 65mm stainless loads

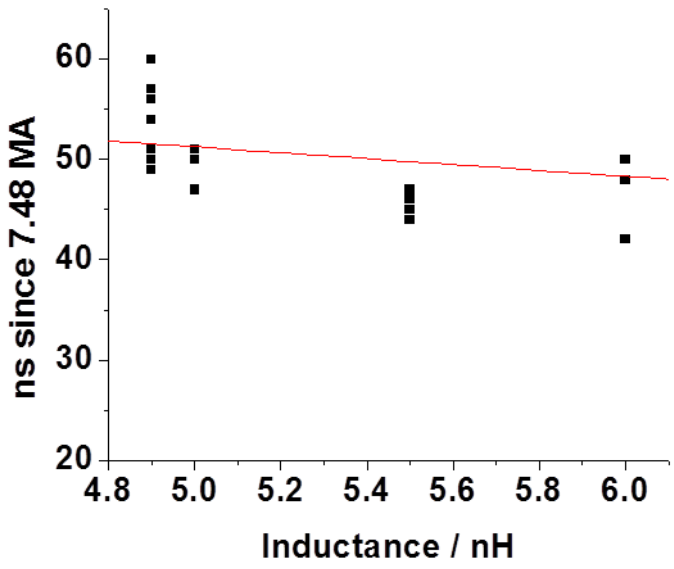

Figure 29. Onset of convolute loss

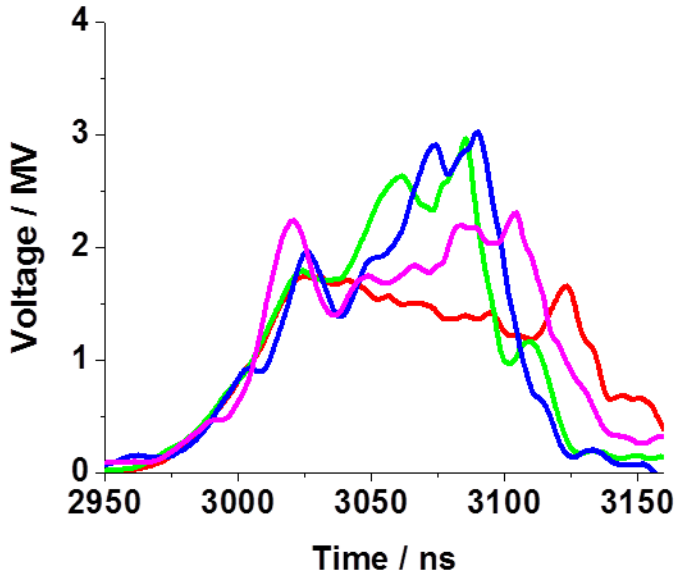

Figure 30. Convolute voltages corresponding to convolute losses

5. APPLICATION TO MODELING LOADS ON Z

The GORGON code is a fixed grid, eulerian, finite volume code. The calculations we discuss here were modeled with 150 micron cell size, modeling the full circumference and full height of each wire array. Discrete wires are initialized as single cell regions of cold dense vapor. This approach has been used successfully to reproduce the ablation structure experimentally observed in which a cold dense wire core serves as a mass source. Material is ablated from these cores, and accelerated by the magnetic field towards the array axis. When the wire cores are sufficiently depleted, the wire cores break up and the array implodes. This setup lacks the resolution to self consistently reproduce the axial variation in this ablation structure that ultimately seeds the Magneto-Raleigh-Taylor instabilities that disrupts the implosion [11]. We therefore apply a randomly modulated, sinusoidal axial mass variation to the initial wire cores with a ~2% amplitude, around a wavelength based on experimentally observed mass variations. Logarithmic mass density plots of a typical, large diameter stainless steel wire array implosion are shown in Figure 31. Typical density plots for the implosion of large diameter stainless steel wire array.

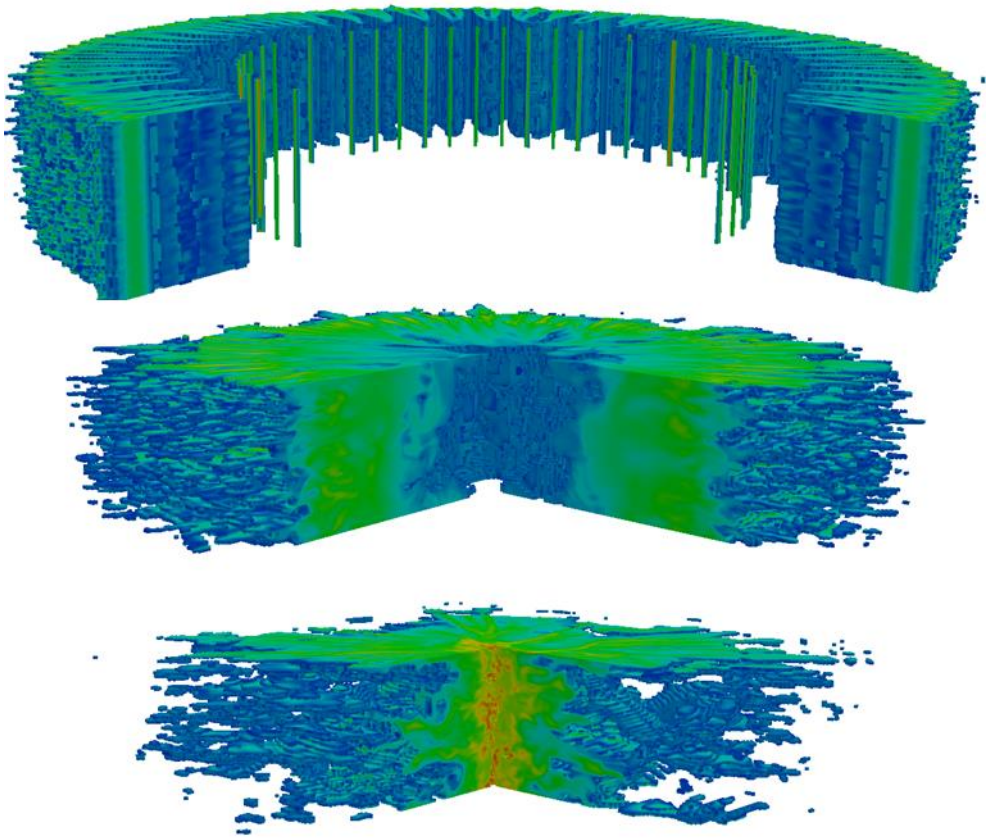

Figure 31. Typical density plots for the implosion of large diameter stainless steel wire array.

Using a circuit model derived from the profiles described in section 3, and the convolute loss resistances described in section 4, we can attempt to drive these MHD simulations of the load

implosions with a realistic representation of the convolute current loss. However, previous results on compact tungsten wire arrays found that consistency between electrical data and load performance could only be found with the assumption of an additional, undiagnosed current loss in the power feed connecting to the load. That work assumed an electron flow current loss, but suggested no physical mechanism for how that current loss may develop and operate.

For a 70mm diameter stainless steel load Figure 32 shows the power feed that connects the convolute to the load. Because of the large initial array diameter this feed is very short. Given the location of the load current monitor next to the convolute anode post, any current loss in the final feed would simply be regarded as current in the load. The presently accepted mechanism for current loss in the convolute is plasma collecting in the cathode post hole expanding across the gap and connecting with the anode post in the location indicated in Figure 32. When current is carried by plasma in this location it will be accelerated upwards towards the load. Given our acceptance that plasma can collect and form in the convolute and form a multi-MA current loss, it seems reasonable to assume that a comparable loss might be formed if a low density plasma was able to collect between a comparable anode-cathode gap further downstream. Specifically, if low density plasma, ejected from the convolute were to collect in the feed that connects to the load we might form an additional and comparable resistive loss in this location. This would assume that the additional current loss in the feed would begin at roughly the same time as the convolute current loss.

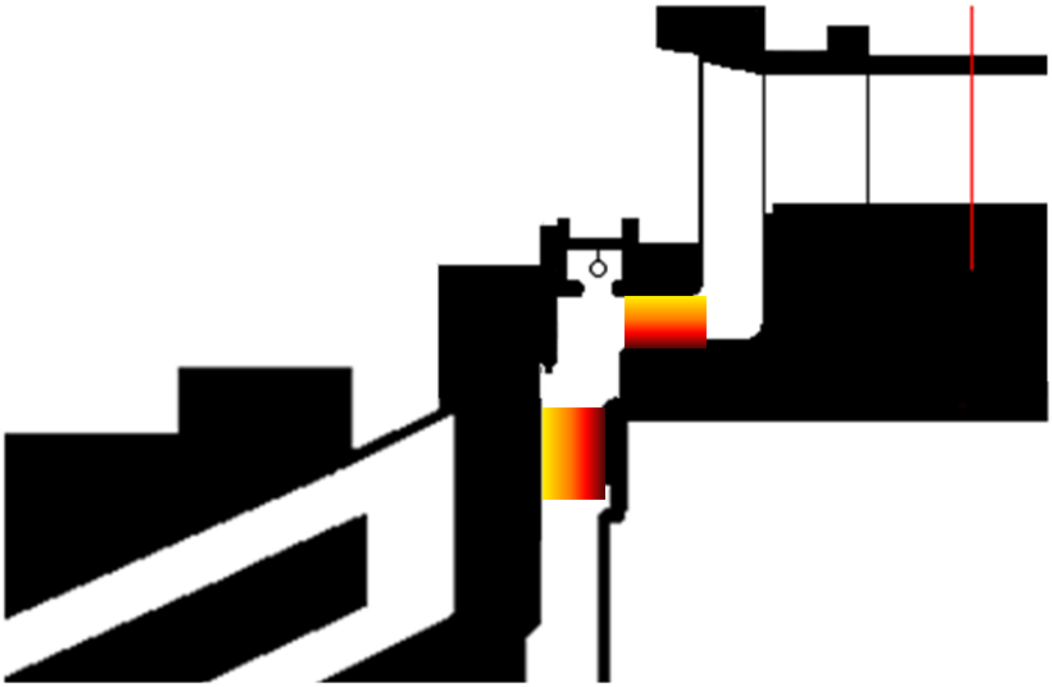

Figure 32. Convolute and feed section

To allow for this kind of current loss we modify the circuit connecting to the load by including an additional resistance to ground separated from the convolute loss resistance by the inductance of the top section of the convolute. We assume that the feed loss follows the behavior of the convolute current loss. Specifically, we assume that the resistive loss "turns on" in a similar way, and then decays to a fixed resistance, we simply assume that the feed loss is the convolute loss multiplied by a constant scaling factor. Applying this to our circuit/MHD model, we can modify this scaling factor to try and better match the experimental electrical data.

5.1. Low mass 70mm stainless steel wire arrays

We start with the 70mm diameter stainless steel wire array described in section 4 (specifically shot Z2236), using the convolute loss that was characterized for this shot. Figure 33 compares the simulated stack and load currents with the measurements. Agreement is generally good throughout the current rise. The structure seen in the differences between stack and load currents at early time are the result of finite propagation times down the 4 different length transmission lines. Reproducing this structure highlights the advantage of using a circuit model that can accommodate these finite propagation time effects.

While we agree through peak current, in the final stages of implosion, to prevent our simulated currents dropping too quickly compared to the experiment, we allow for a small amount of additional current loss in the final feed. This effect is small for this load, for reasons that will become apparent in subsequent comparisons we include it at this stage.

For our large diameter stainless steel array the feed loss was calculated from the convolute loss using a scaling factor of 3.3 to produce currents shown in Figure 33. In addition to the load and stack currents we also show a convolute current that represents the current as seem at the b-dot location. i.e the current measured between the convolute current loss and the feed current loss. The stack current definition remains unchanged, and the load current still refers to the current actually flowing in the wire array or liner load.

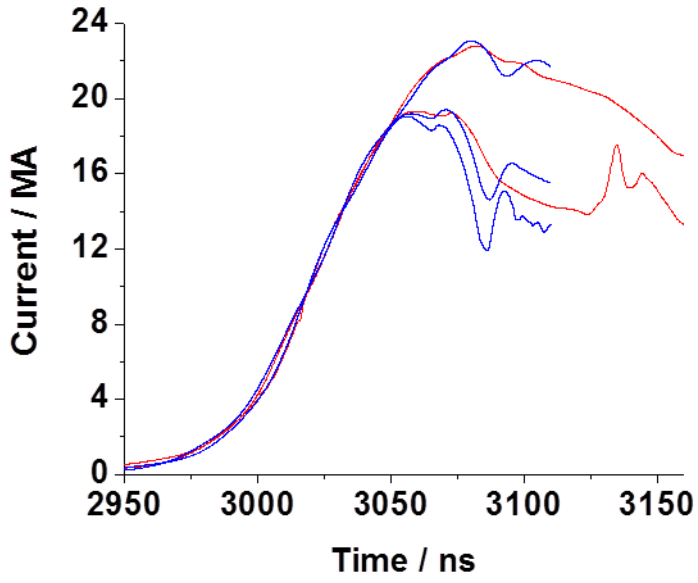

Figure 33. Current Comparison for stainless steel 70mm shot Z2236

5.2. 65mm Stainless Steel Load

We now compare simulated and measured stack and load currents for the heavier 65mm stainless steel wire arrays discussed in section 4. Specifically we model shot 1860. Neglecting the feed loss, and applying only the convolute current loss the comparison between measured and simulated currents is shown in Figure 34. The discrepancy hinted at in the 70mm stainless steel array is now much more apparent. Introducing an additional feed loss, which we again calculate as the convolute resistance multiplied by a scaling factor, we find a scaling factor of 1.4 results in the currents shown in Figure 35. Current Comparison with additional feed loss stainless steel 65mm shot Z1860. Agreement is significantly improved, where we now require an additional ~4.5MA of current loss at stagnation to provide consistent agreement with the electrical data.

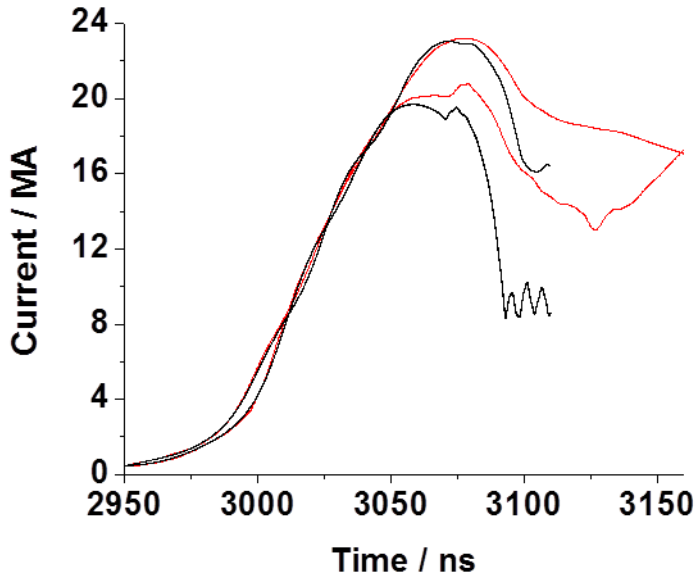

Figure 34. Current Comparison for stainless steel 65mm shot Z1860

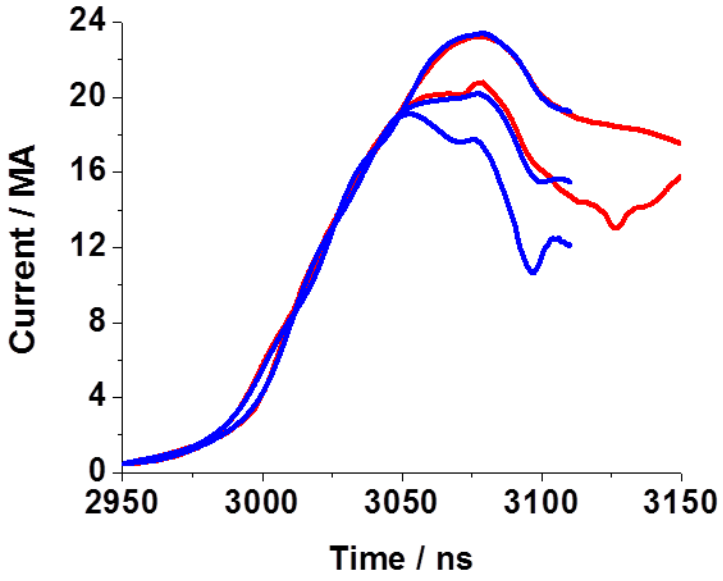

Figure 35. Current Comparison with additional feed loss stainless steel 65mm shot Z1860

It is conceivable that these differences in current delivery actually reflect some aspect of the implosion and stagnation not adequately captured by the MHD model. It is however interesting

to note that relatively dramatic changes to the implosion physics have little effect of the electrical response of the load. As an example we can compare a 3D full volume MHD calculation, with a 2D shell like implosion. The 2D calculation models the implosion in a plane perpendicular to the array wires, so is able to reproduce the same wire ablation behavior as the 3D calculation, but since it assumes axial uniformity it does not allow for the development of MRT instabilities. As a result, we have a much more uniform, shell like implosion. Density profiles from these two calculations are shown in Figure 36, and the electrical behavior is compared in Figure 37.

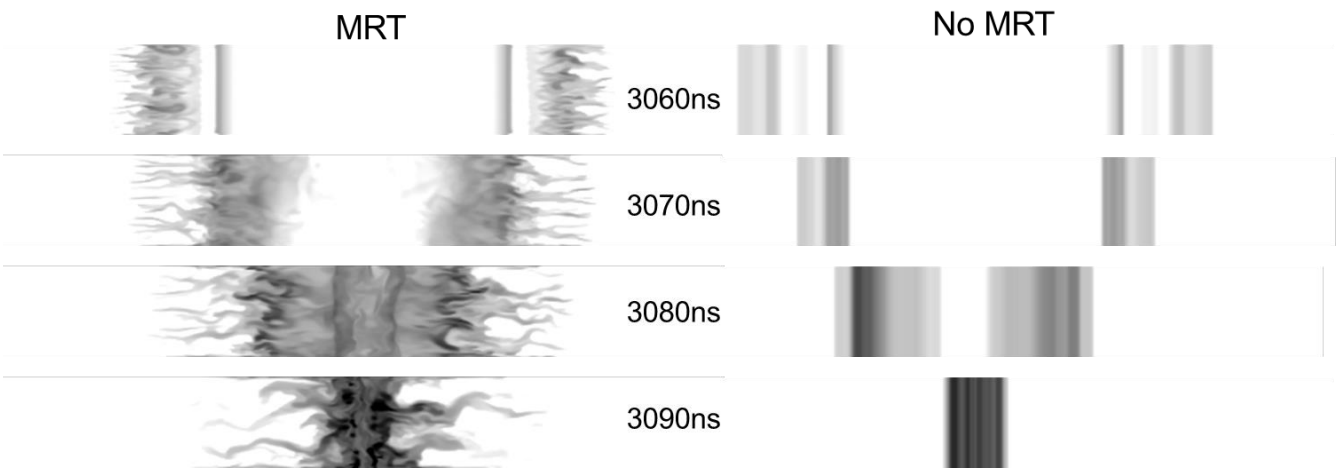

Figure 36. Density profiles 2D vs. 3D

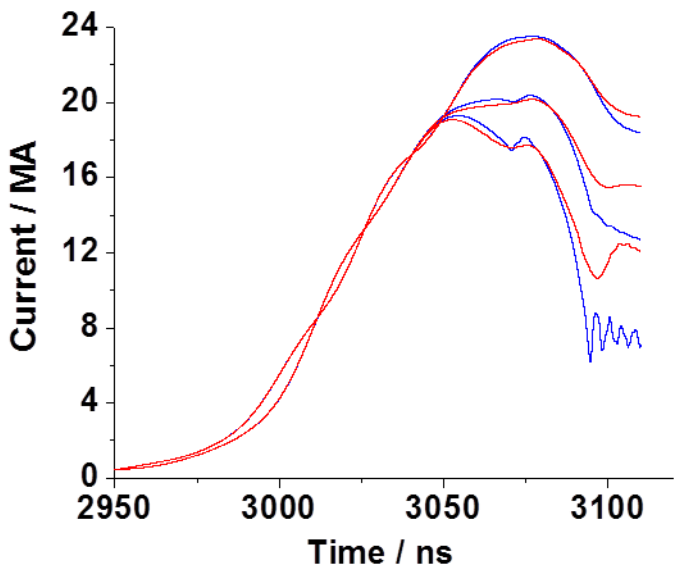

Figure 37. Comparison of currents between 2D (blue) and 3D (red)

While this is an extreme example it does illustrate a certain insensitivity of the circuit response to the details of the implosion physics, and provide us some confidence that discrepancies between

currents delivered may lie elsewhere. Certainly modifications to some of the assumptions made in the physics models can affect little change to the final circuit response. The circuit response is mainly a reflection of the implosion trajectory, and as such it is, to first order, simply a reflection of the mass imploded by the force applied.

Energetically this simulation produced a total yield of 1.5MJ in the main x-ray pulse, which is still consistent with the ~1.4MJ experimentally measured in the main pulse. (Although we note that this experiment radiated an additional 0.4MJ in a long tail to the power measurements which extended beyond the end of our simulation). A K-shell yield of 26kJ was recovered in this shot, which was low compared to experimental results of 34 – 47kJ recovered in experiments with this configuration. That is not however unusual for calculations run at the relatively coarse resolution of 150microns used here. If we neglect the feed loss, then the total yield can rise by ~15%, but the K-shell yield can be as much as ~50% higher. High photon energy emission is considerably more sensitive to changes in the temperature, so does stand to benefit if more kinetic energy can be supplied to the plasma in the final stages of implosion.

5.3. 65mm Copper load

Remaining with 65mm diameter arrays we can now compare a very similarly massed copper wire array, discussed in section 4. Specifically Z shot 1975. For this implosion we find that a convolute resistance scaling factor of 2.5 is required to model the feed loss and match to the electrical data. This indicates less of a final feed current loss than evident in the similarly massed stainless steel implosion. This is partly evident in the experimental b-dot measurements themselves, where the copper current signal is pulled lower, later in the implosion. This is indicative of a higher voltage at the load. For an otherwise identical implosion, this would indicate a higher current reaching the actual load region. The copper wire arrays did have a lower wire number, which may have altered implosion symmetry, but given the large initial array radius they are all in the limit of large inter-wire gaps to initial wire diameters. i.e. they can all be expected to ablate as discrete wires without merging into a more azimuthally uniform shell. The other difference that distinguishes the copper wire array implosion from the stainless steel and tungsten implosions, was a redesign to the final feed that connects to the load. This will be discussed in more detail later, but the fact a different feed design has resulted in a different required feed current loss is potentially revealing.

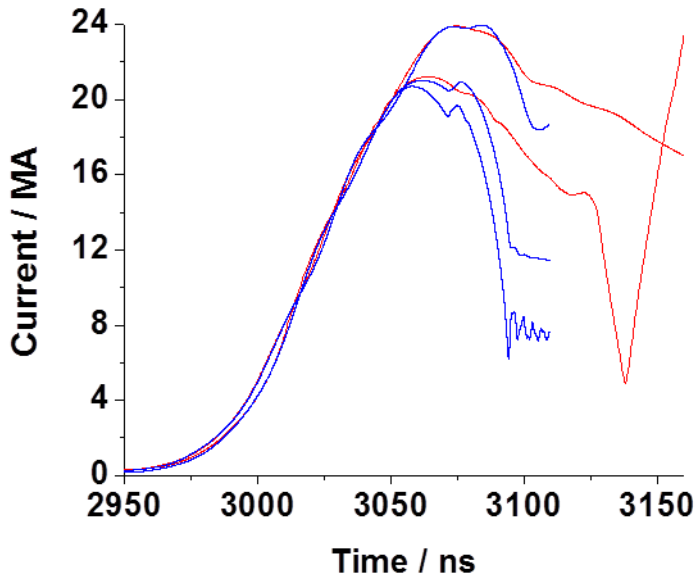

Figure 38. Comparison of currents Z1975 Copper Array

5.4. 50mm Aluminum Load

Progressing to smaller initial array radius we now compare simulated and measured stack and load currents for the 50mm, Aluminum wire arrays. In this instance we find we need a feed loss scaling factor of 2 to reproduce the electrical performance seen through comparison with the load currents.

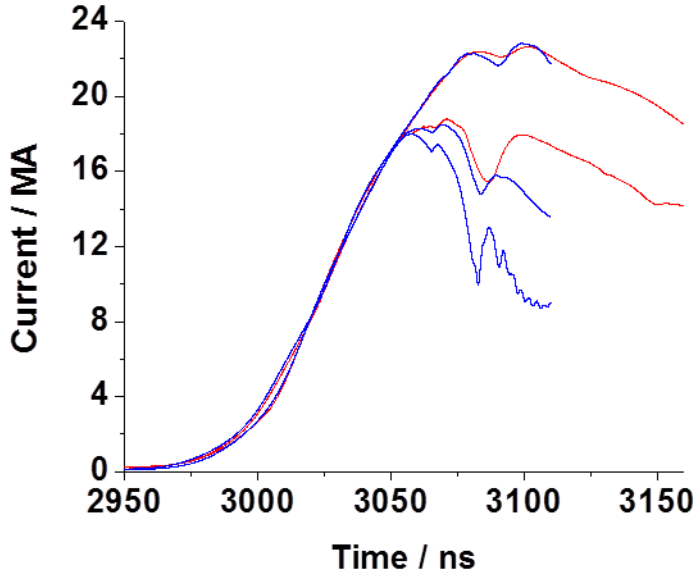

Figure 39. Comparison of currents Z2337 Aluminum Array

5.5. 40mm Dynamic Hohlraum Load

Modeling the 40mm diameter dynamic hohlraum loads we again find similar behavior, with a feed loss scaling factor of 1 is now required to match to the electrical measurements as seen in Figure 40 for two different masses corresponding to Z shots 2299 and 1898

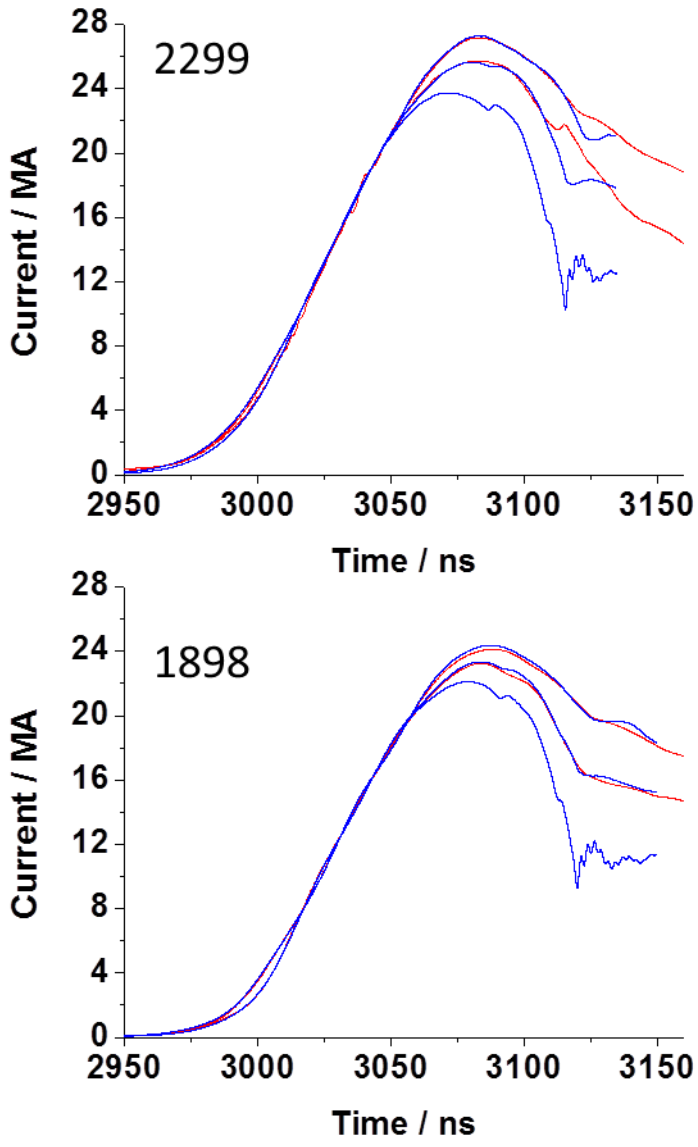

Figure 40. Comparison of currents for dynamic hohlraum loads

5.6. Correlation of feed loss performance with hardware geometry

Given that different scaling factors are required to rescale the convolute loss to provide the necessary amount of feed loss, we can compare these scaling factors for the different feed geometries fielded. This is shown in

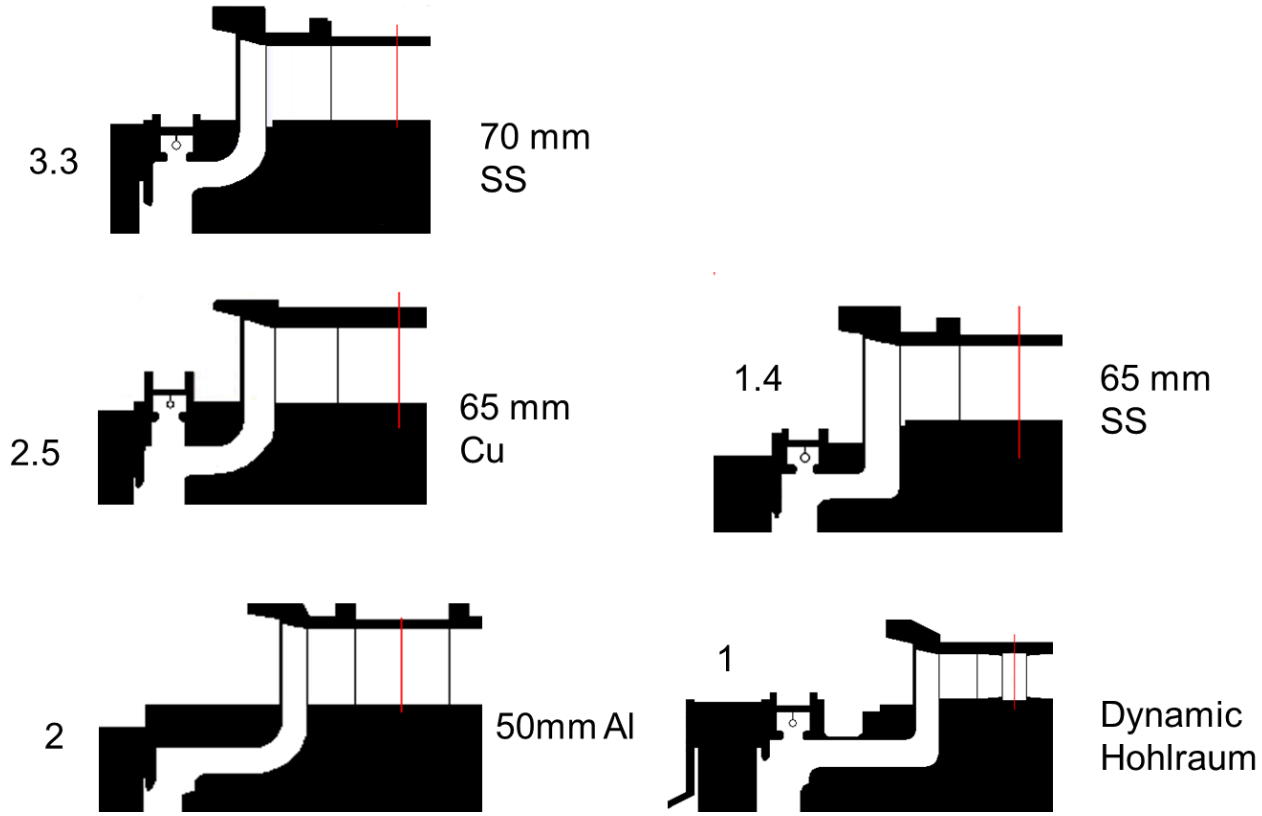

Figure 41. Feed loss profile compared to convolute loss scaling factor

Higher scaling factors are indicative of smaller feed losses. In general we find that the amount of feed loss requires, increases for increasing feed length. Additionally, feed loss appears to be exacerbated by a tight radius of curvature in the transition from horizontal to vertical feeds where the load height is raised. If plasma is moving into the feed section this indicates that certain geometries may make the resulting current loss worse.

5.7. MagLif Beryllium Liners

We now turn our attention to simulations of the MagLif style, small diameter beryllium liners. We consider two different configurations which utilize two different power feed designs. As previously noted in section 4 these loads exhibited convolute loss behavior unlike the previous wire array implosions. Furthermore, as the feed inductance was increased the current loss appeared to get considerably worse. Previous simulations of the implosion of these liners have demonstrated good agreement between the density distributions simulated and those measured through radiography of the imploding load [20]. This gives us some confidence that we can

accurately simulate these loads, and reproduce the MRT instability structures that disrupt these implosions.

Beginning with the lower inductance power feed (Z shots 2105 and 2172 discussed in section 4) we can take the experimentally determined convolute loss resistance and use it to drive a simulation of the liner implosion. For these calculations we neglect any additional power feed losses. This results in the stack and load currents shown if Figure 42.

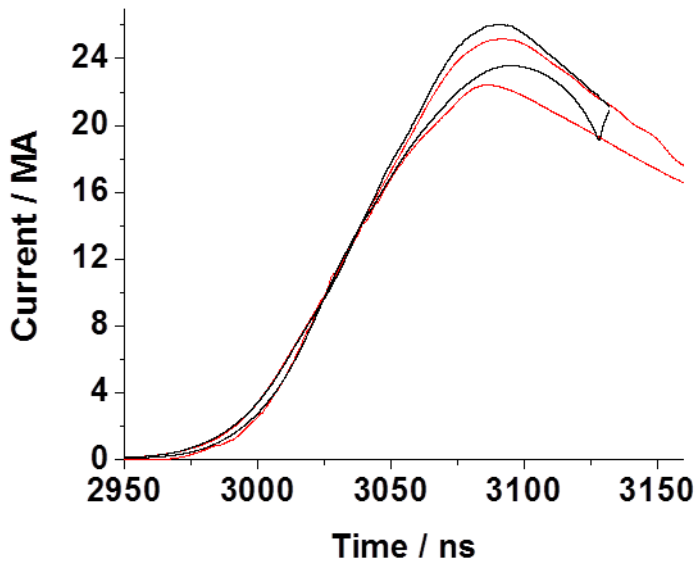

Figure 42. Liner driven with measured convolute loss

The implosion of the wire array loads typically resulted in simulated currents lower than measurements, as the high implosion voltage drove significant current losses. If these losses were not properly accounted for too much current reached the load region, driving an anomalously high voltage, which pulled the simulated currents down low. Our simulated liner implosions seem to be having the opposite problem. When we assume the convolute loss resistance calculated from the experiment, too little current appears to be reaching the load. The late time load voltage is not high enough, allowing the generator to deliver too much current to the load. The simulated stack and load currents are therefore coming in too high, as shown in Figure 42. If instead of using the circuit model and measured convolute loss, we now drive our load calculation with the measured convolute voltage, we will drive a current through the load that is consistent with that voltage.

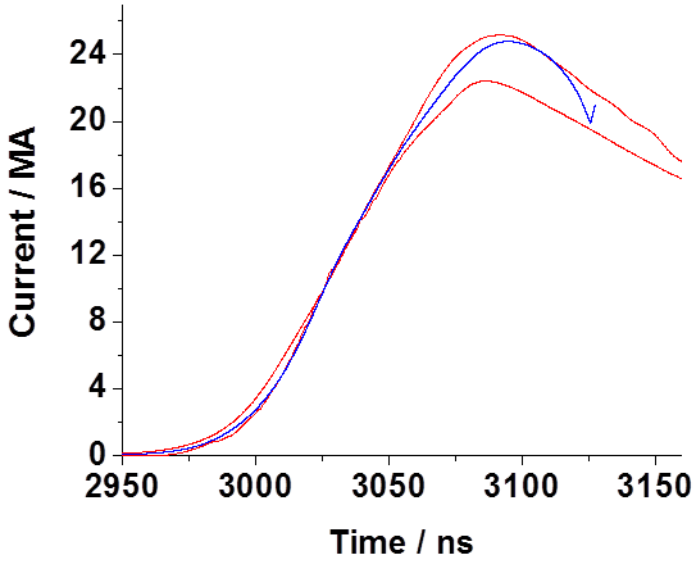

Figure 43. Voltage driven liner calculation

This load current is shown if Figure 43, and is seen to be significantly higher than the current measured at the exit to the convolute. This implies that for the load calculation to be consistent with the stack voltage and current measurements, the b-dot at the convolute must not be representative of the current delivered to the liner. Previous simulation work by D. Rose [17] has indicated that in some situations b-dots in the vicinity of the convolute can be struck by electron flow electrons which can result in poor signals. Looking in more detail at the load b-dot signal, at late time it clearly rises far above the stack current. At this point it has obviously failed. At earlier times, in the simulated load current there is a clear signature of the stagnation of the array on axis. In the stack voltage measurements (Figure 22) this is discernible as a small rise in the voltage. It is therefore suspicious that there is no discernible feature in the measured load current at this time. We instead assume the b-dot measurement is in error, and that the simulation driven by the measured voltage is accurately reproducing the true load current. From the measured stack current, stack voltage, and simulated load current we can therefore attempt to reconstruct what the convolute loss resistance should have been for this shot. This is shown in Figure 44, where it is compared to "measured" convolute resistance discussed in section 4, and to the convolute resistance taken from one of the dynamic hohraum loads.
In section 4 the convolute resistance from this liner implosion was unusual in that it didn't seem to fit the pattern established by other imploding loads. If we instead use a load current that is consistent with both the simulated liner implosion, and the measured stack voltage, then we actually find that the convolute resistance closely follows the pattern established by the other imploding loads.

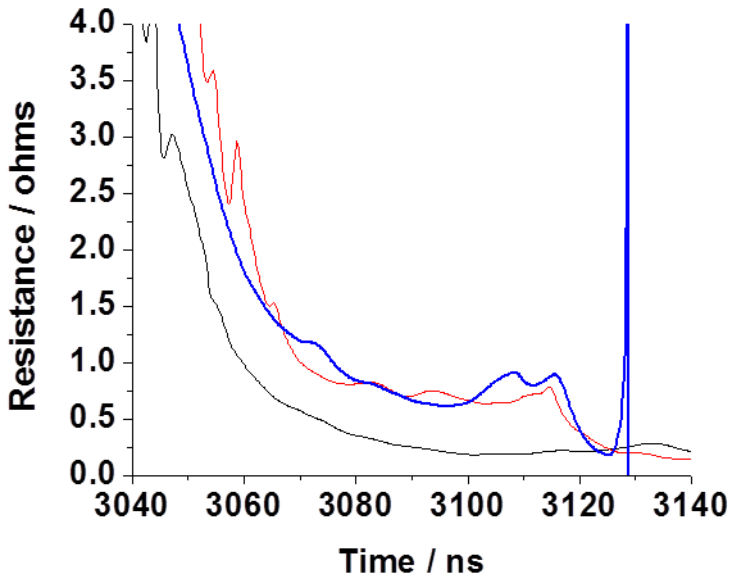

Figure 44. Reconstructed convolute resistance (blue), measured resistance (black), dynamic hohlraum resistance (red)

In fact, we find that consistency between stack measurements and load simulation implies that the current delivery to these loads is excellent, which for these loads is not surprising. It is true that the initial inductance of these small diameter liners is high, but at this time the convolute resistance has not collapsed. At later times the convolute voltage has dropped considerably (Figure 22). With these slowly imploding liners there is little contribution to the voltage from the rate of change of inductance. The fixed inductance is high throughout, but only contributes significantly to the voltage when the rate of change of the current is high at the start of the current rise. As the liner implodes, the voltage over the convolute is low, so if the convolute resistance was behaving in the same way as other experiments, then the resulting current loss would be very small. It is partly for this reason that we do not attempt to include any additional power feed current loss. If an additional loss, similar to those inferred on other experiments, were located in the feed, then the voltage is probably too low to drive a meaningful current through it.

We apply a similar analysis to the shot which used the higher inductance, raised power feed [19]. Simple comparison of the measured load currents between these lower and higher inductance feeds implies that a small, ~0.8nH increase in the initial inductance has created a large difference in convolute performance. (Figure 22 and Figure 24) Driving a simulation of this liner implosion with the convolute resistance measured from this experiment results in a larger discrepancy between measured and simulated currents as shown in Figure 45. If we instead assume the convolute performance is standard across all these loads then the resulting simulated stack and load currents are shown in Figure 46. The stack current now more closely follows the measurement, and the current delivery to the load is again excellent. Comparing the simulated and measured convolute voltages finds they are also in good agreement (Figure 47), indicating this choice of current delivery and convolute resistance is also consistent with the stack voltage measurements.

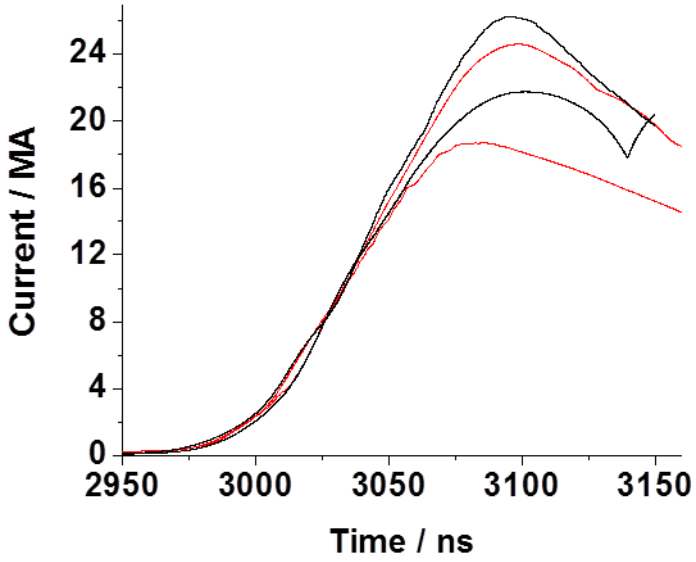

Figure 45. High initial inductance liner calculation using measured convolute loss

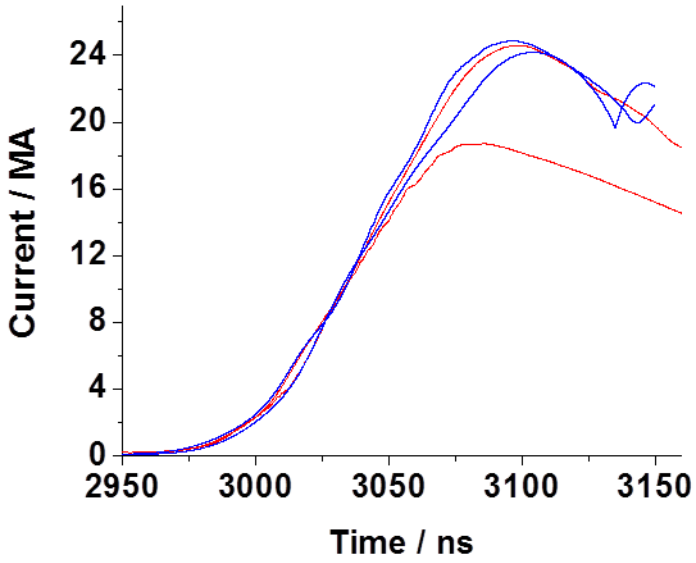

Figure 46. High initial inductance liner calculation using standard convolute loss

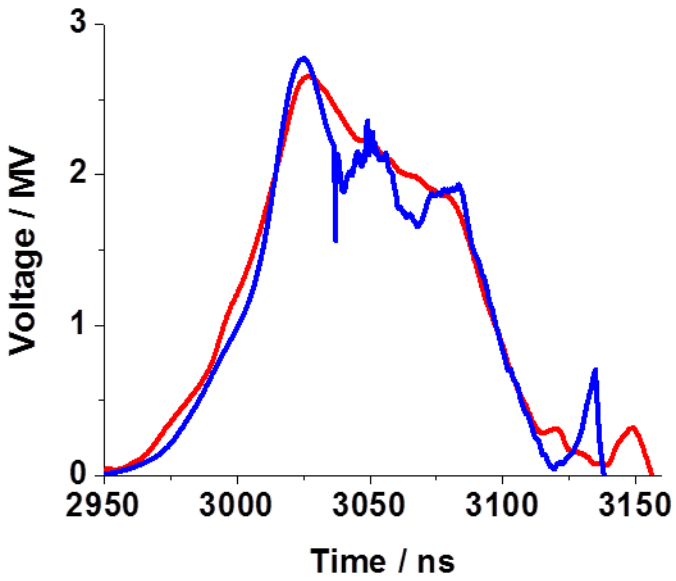

Figure 47. High initial inductance liner voltage using standard convolute loss

This implies that the small increase in initial load inductance resulting from raising the power feed, made very little difference to the convolute performance, or current delivery to the load. This conclusion is actually supported by just examining the data. If we compare stack voltages and currents between the lower and higher inductance feeds then we find they agree closely (Figure 48). If the convolute loss were significantly worse for the raised power feed then we would expect the stack current to be higher, as the generator essentially sees something that looks more like a short circuit. When convolute loss increases it is not just the load current that goes down, the stack current would also increase in response to this. The fact that this does not occur further indicates that we likely have a problem with the current measurement at the exit to the convolute.

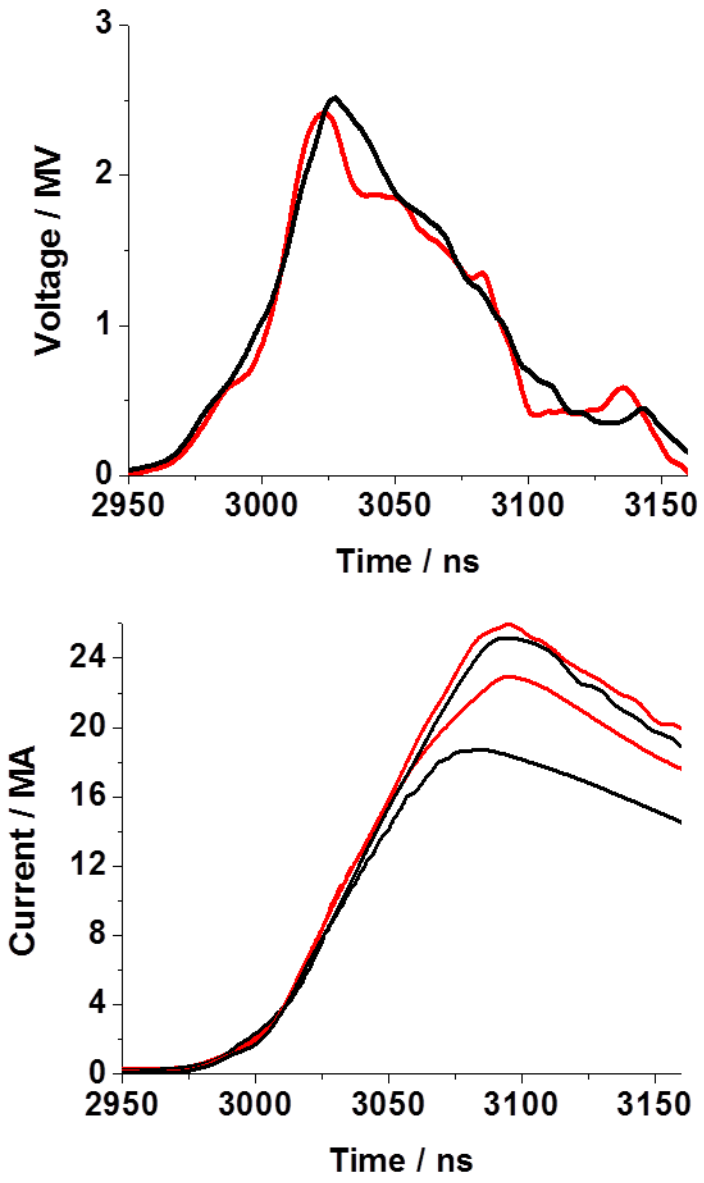

Figure 48. Stack and convolute current and voltage measurements for lower (red) and higher (black) inductance liner feeds

5.7. Gas Puffs

We specifically examine the implosion of a Kr gas puff fielded by David Ampleford, although the conclusions seem applicable to other gas puff loads that have been fielded on Z. These 8cm diameter gas puffs are the largest loads that can be fielded in the convolute we discuss here. For the Krypton shot (Z2383) multiple different styles of B-dot were fielded resulting in a large

spread in possible load currents. Again we appeal to simulations, and drive an MHD simulation of the load with the measured convolute voltage, to recover a load current consistent with that voltage. This is shown as the black line in Figure 49.

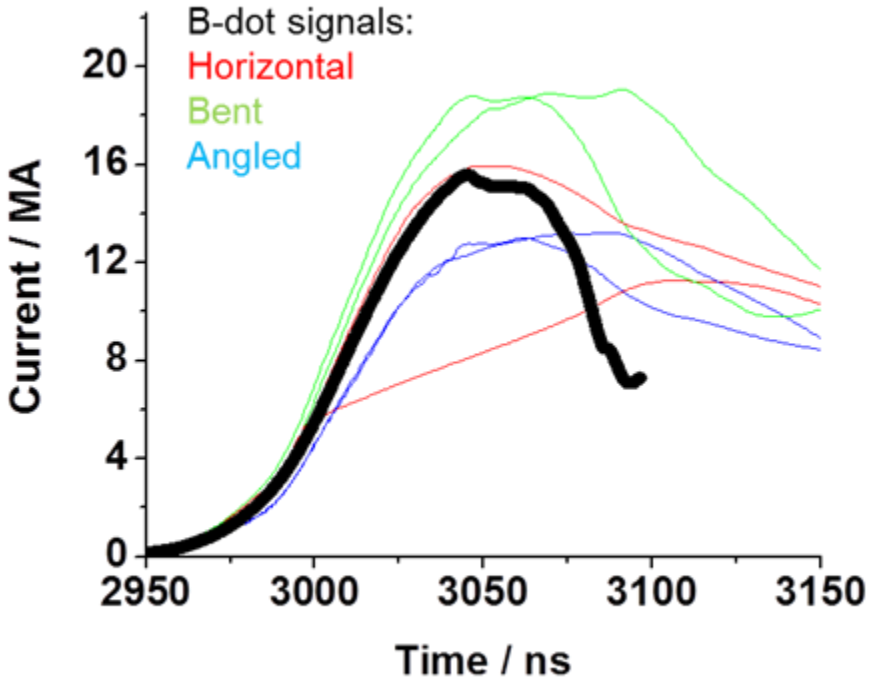

Figure 49. Current delivery to Kr gas puff

Picking the b-dot that most closely agreed with this signal we constructed the convolute loss resistance previously discussed. This convolute resistance appears significantly lower than measured for the wire array loads, or now inferred in the liner loads. It is however consistent with simulation results, convolute and stack measurements, and one of the b-dot styles fielded. It should be noted that the larger current signals here actually rise significantly above the translated stack current measurements, indicating a potential calibration issue with this style of B-dot. Furthermore, the lower current delivery indicated by the simulations, still provides radiated yields consistent with experiment. It is therefore possible, that for the gas puff loads fielded so far, the convolute performance is actually worse than for other loads on Z. Examining the hardware for this shot in Figure 50, possible reasons for this may be associated with the large initial gas puff diameter.

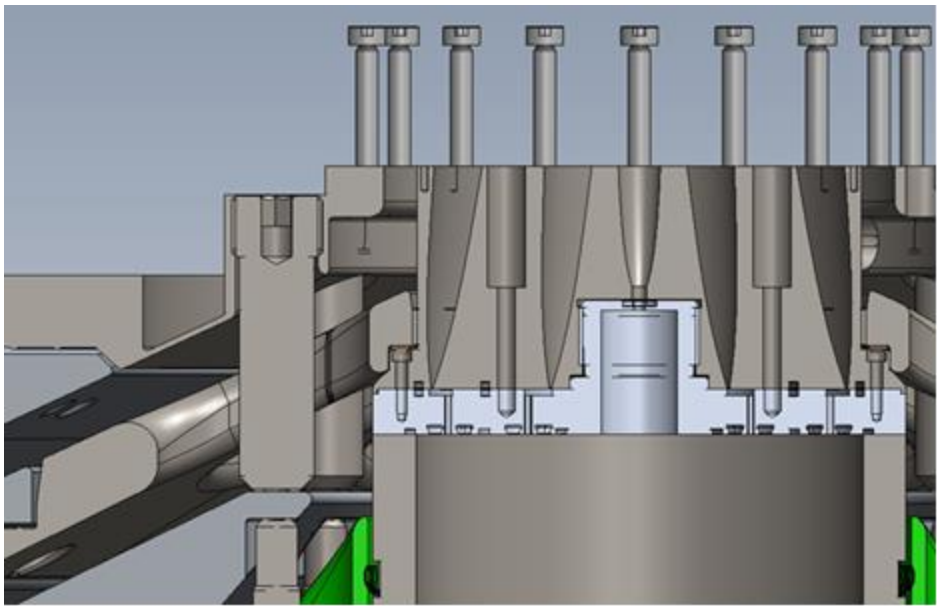

Figure 50. Gas puff connection to convolute

The outside edge of this load sits on the edge of the convolute, and has a direct line of sight down into the convolute. Radiation from the initial breakdown and the start of the implosion of the gas puff may be able to directly irradiate the convolute, ultimately resulting in a higher convolute loss. Alternatively, gas from the puff itself may be able to drift into parts of the convolute. It is hoped that more data from subsequent experiments will resolve further our understanding, but the initial interpretation is that current losses and convolute performance are worse for these shots.

6. CONCLUSIONS

Through requiring consistency between load calculations and generator electrical diagnostics we arrive at the following conclusions:

1 - Behavior of the Convolute is consistent and reproducible for short pulse Z experiments, maintaining the same resistance despite large differences in voltage and current loss.

2 - Additional Current losses may be present in the inner MITL feed.

3 - The B-dots used in liner experiments may not be accurately representing the late time current delivery.

4 - Current delivery to MagLif liner targets is very good, consistent with its low, late time load voltage.

5 - The convolute is able to robustly support high initial inductance liner loads.

6 - Existing gas puff experiments seem to exhibit poor convolute performance and high current losses.

From comparison of a number of different loads on Z, it seems reasonable to conclude that the behavior of the convolute is robust and reproducible. For the implosion of many wire array loads, a reproducible convolute does not necessarily guarantee you can accurately determine the current delivered to the load. While it is always desirable to be able to separate a problem into discrete parts, with regards to the convolute and inner MITL feed this may not be possible. Many results are consistent with an additional current loss in the system. It has been postulated here that this additional loss may result from plasma in the convolute migrating further into the power feed. We generally accept that low density plasma can create a short in the convolute able to support several MA of current. JxB acceleration of this low density convolute plasma would likely direct it towards the power feed, which is a very short distance from the convolute loss location. It does not seem unreasonable to conclude that plasma driven current losses may be more prevalent, and not solely confined to one convolute location. However, there currently exists no direct experimental confirmation of the existence such plasma. Given apparent correlations between power feed design, and the magnitude of additional loss, a straightforward test could be conducted by reshaping the power feed to a dynamic hohlraum load. Hopefully we would affect some change in the electrical data returned. While additional loss would unlikely be eradicated, if a difference were observed it could confirm the existence of some loss in the power feed.

Current measurements made for the high initial inductance liner loads seem inconsistent with simulated load voltages. If these current measurements are indeed questionable, then the convolute performance for these shots is consistent with the convolute performance for many other shots with comparable voltage time histories. If this is true, then we may have

underestimated the initial load inductance that the convolute can support, and may have more flexibility to increase the load inductance of these loads if necessary.

Based on an extremely limited number of shots, the convolute performance for large diameter gas puff loads does appear to be worse. This may be indicative of either gas, or radiation making it into the convolute. Given the large initial load diameter, and an essentially clear line of sight between load and convolute, this does seem plausible. If poor current delivery is observed in subsequent shots then some redesign of the gas puff loads to better separate the load and convolute may be beneficial.

REFERENCES

1. C. Harjes, J. Elizondo, K. Struve, L. Bennett, D. Johnson, and B. Shoup, “Circuit modeling for ZR,” in Proc. 14th IEEE Int. PPC, 2003, pp. 917–920.

2. Jennings, C.A. et al, " Simulations of the implosion and stagnation of compact wire arrays," Phys. Plasmas 17, 092703 (2010)

3. Rose, D.V.; Welch, D.R.; Clark, R.E.; Madrid, E.A.; Miller, C.L.; Mostrom, C.; Stygar, W.A.; Cuneo, M.E.; Jennings, C.A.; Jones, B.; Ampleford, D.J.; Struve, K.W., "ZR-convolute analysis and modeling: Plasma evolution and dynamics leading to current losses," Pulsed Power Conference, 2009. PPC '09. IEEE , vol., no., pp.1153,1158, June 28 2009-July 2 2009

4. Jennings, C.A. et al "Circuit Model for Driving Three-Dimensional Resistive MHD Wire Array Z -Pinch Calculations," IEEE Transactions on Plasma Science, Volume: 38 , Issue: 4 Page(s): 529 - 539 April 2010

5. McBride, R.D. et al "Displacement current phenomena in the magnetically insulated transmission lines of the refurbished Z accelerator" Physical Review Special Topics - Accelerators and Beams 13, 120401 (2010)

6. K.W. Struve, T. H. Martin, R. B. Spielman,W. A. Stygar, P. A. Corcoran, and J. W. Douglas, “Circuit-code modeling of the PBFA Z for Z-pinch experiments,” in Proc. 11th IEEE Pulsed Power Conf., G. Cooperstein and I. Vitkovitsky, Eds., Baltimore, MD, 1997, pp. 162–167

7. W. A. Stygar, R. B. Spielman, G. O. Allshouse, C. Deeney, D. R. Humphreys, H. C. Ives, F. W. Long, T. H. Martin, M. K. Matzen, D. H. McDaniel, C. W. Mendel, Jr., L. P. Mix, T. J. Nash, J. W. Poukey, J. J. Ramirez, T. W. L. Sanford, J. F. Seamen, D. B. Seidel, J. W. Smith, D. M. Van De Valde, R. W. Wavrik, P. A. Corcoran, J. W. Douglas, I. D. Smith, M. A. Mostrom, K. W. Struve, T. P. Hughes, R. E. Clark, R. W. Shoup, T. C. Wagoner, T. L. Gilliland, and B. P. Peyton, “Design and performance of the Z magnetically-insulated transmission lines,” in Proc. 11th IEEE Int. Pulsed Power Conf., Dig. Tech. Papers, Jun. 29–Jul. 2, 1997, vol. 1, pp. 591–596.

8. M. E. Savage, “An overview of pulse compression and power flow in the upgraded Z pulsed power driver,” in Proc. 16th IEEE Pulsed Power Conf., E. Schamiloglu and F. Peterkin, Eds., Albuquerque, NM, 2007, pp. 979–984.

9. T. C. Wagoner, W. A. Stygar, H. C. Ives, T. L. Gilliland, R. B. Spielman, M. F. Johnson, P. G. Reynolds, J. K. Moore, R. L. Mourning, D. L. Fehl, K. E. Androlewicz, J. E. Bailey, R. S. Broyles, T. A. Dinwoodie, G. L. Donovan, M. E. Dudley, K. D. Hahn, A. A. Kim, J. R. Lee, R. J. Leeper, G. T. Leifeste, J. A. Melville, J. A. Mills, L. P. Mix, W. B. S. Moore, B. P. Peyton, J. L. Porter, G. A. Rochau, G. E. Rochau, M. E. Savage, J. F. Seamen, J. D. Serrano, A. W. Sharpe, R. W. Shoup, J. S. Slopek, C. S. Speas, K. W. Struve, D. M. van de

Valde, and R. M. Woodring, “Differential-output B-dot and D-dot monitors for current and voltage measurements on a 20-MA, 3-MV pulsed-power accelerator,” Phys. Rev. ST Accel. Beams, vol. 11, no. 10, p. 100401, Oct. 2008

10. J. P. Chittenden, S. V. Lebedev, S. N. Bland, F. N. Beg, and M. G. Haines, “One-, two-, and three-dimensional modeling of the different phases of wire array Z-pinch evolution,” Phys. Plasmas, vol. 8, no. 5, pp. 2305–2314, May 2001.

11. J. P. Chittenden and C. A. Jennings, “Development of instabilities in wirearray Z pinches,” Phys. Rev. Lett., vol. 101, no. 5, p. 055005, Aug. 2008.

12. E. P. Yu, M. E. Cuneo, M. P. Desjarlais, R. W. Lemke, D. B. Sinars, T. A. Haill, E. M. Waisman, G. R. Bennett, C. A. Jennings, T. A. Mehlhorn, T. A. Brunner, H. L. Hanshaw, J. L. Porter, W. A. Stygar, and L. I. Rudakov, “Three-dimensional effects in trailing mass in the wirearray Z pinch,” Phys. Plasmas, vol. 15, no. 5, p. 056301, May 2008.

13. J. P. Chittenden, S. V. Lebedev, C. A. Jennings, S. N. Bland, and A. Ciardi,” X-ray generation mechanisms in three-dimensional simulations of wire array Z-pinches” Plasma Phys. Controlled Fusion 46, B457 _2004

14. Shoup, R.W.; Savage, M.E.; Elizondo, J.M.; Bennett, L.F.; Stygar, W.A.; Harjes, H.C.; Owen, A.C.; Pointon, T.D.; Pasik, M.; Stoltzfus, B.S.; Struve, K.W.; McDaniel, D.H., "Analysis of the ZR Vacuum Insulator Stack," Pulsed Power Conference, 2005 IEEE , vol., no., pp.505,508, 13-17 June 2005

15. J. E. Bailey, G. A. Chandler, S. A. Slutz, I. Golovkin, P.W. Lake, J. J. MacFarlane, R. C. Mancini, T. J. Burris-Mog,G. Cooper, R. J. Leeper, T. A. Mehlhorn, T. C. Moore, T. J. Nash, D. S. Nielsen, C. L. Ruiz,D.G. Schroen, and W. A. Varnum, “Hot Dense Capsule-Implosion Cores Produced by Z-Pinch Dynamic Hohlraum Radiation” Phys. Rev. Lett. 92, 085002 (2004) .

16. S. A. Slutz, K. J. Peterson, R. A. Vesey, R. W. Lemke, J. E. Bailey, W. Varnum, C. L. Ruiz, G. W. Cooper, G. A. Chandler, G. A. Rochau, and T. A. Mehlhorn, “Integrated two-dimensional simulations of dynamic hohlraum driven inertial fusion capsule implosions” PHYSICS OF PLASMAS 13, 102701 2006 .

17. Rose, D.V et al "10^7-A load-current B-dot monitor: Simulations, design, and performance" Phys. Rev. ST Accel. Beams 13, 040401 (2010)

18. T. D. Pointon,W. A. Stygar, R. B. Spielman, H. C. Ives, and K.W. Struve, “Particle-in-cell simulations of electron flow in the post-hole convolute of the Z accelerator,” Phys. Plasmas, vol. 8, no. 10, pp. 4534–4544, Oct. 2001.

19. R. D. McBride, M. R. Martin, R. W. Lemke, J. B. Greenly, C. A. Jennings, D. C. Rovang, D. B. Sinars,M. E. Cuneo, M. C. Herrmann, S. A. Slutz, C. W. Nakhleh, D. D. Ryutov, J.-P. Davis, D. G. Flicker,B. E. Blue, K. Tomlinson, D. Schroen, R. M. Stamm, G. E. Smith, J. K.

Moore, T. J. Rogers, G. K. Robertson, R. J. Kamm, I. C. Smith, M. Savage, W. A. Stygar, G. A. Rochau, M. Jones,M. R. Lopez, J. L. Porter, and M. K. Matzen, "Beryllium liner implosion experiments on the Z accelerator in preparation for Magnetized Liner Inertial Fusion (MagLIF)" Phys. Plasmas, accepted Feb. 2013

20. R. D. McBride, S. A. Slutz, C. A. Jennings, D. B. Sinars, M. E. Cuneo, M. C. Herrmann, R.W. Lemke,M. R. Martin, R. A. Vesey, K. J. Peterson, A. B. Sefkow, C. Nakhleh, B. E. Blue, K. Killebrew, D. Schroen,T. J. Rogers, A. Laspe, M. R. Lopez, I. C. Smith, B.W. Atherton, M. Savage, W. A. Stygar, and J. L. Porter, "Penetrating Radiography of Imploding and Stagnating Beryllium Liners on the Z Accelerator" PRL 109, 135004 (2012)

21. S. A. Slutz, M. C. Herrmann, R. A. Vesey, A. B. Sefkow, D. B. Sinars, D. C. Rovang, K. J. Peterson, and M. E. Cuneo, "Pulsed-power-driven cylindrical liner implosions of laser preheated fuel magnetized with an axial field" PHYSICS OF PLASMAS 17, 056303 2010

22. D. J. Ampleford, C. A. Jennings, B. Jones, C. A.Coverdale, T.J. Nash, S. C. Jones, M.C. Jones, W. A. Stygar, M. E. Savage, K. R. LeChien, S.B. Hansen, M. E. Cuneo, J. W. Thornhill, J. L. Giuliani, J. P. Apruzese, R. W. Clark, Y. K. Chong, A. Dasgupta "DEVELOPMENT OF AN 85KJ STAINLESS STEEL K-SHELL X-RAY SOURCE ON THE Z GENERATOR" Presented ICOPS 2010

23. D.J. Ampleford, S.B. Hansen, C.A. Jennings, B. Jones, G.A. Rochau, J. Bailey, A.R. Laspe, M.E. Savage, M.E. Cuneo, R. Clark, Y.K. Chong, J. Apruzese, J.L. Giuliani "Aluminum wire array experiments on the Z generator" Presented at APS 2012

24. M. R. Gomez, M. E. Cuneo, R. D. McBride, G. A. Rochau, D. J. Ampleford, J. E. Bailey, A. D. Edens, B. Jones, M. Jones, M. R. Lopez, M. E. Savage, D. B. Sinars, W. A. Stygar, R. M. Gilgenbach "SPECTROSCOPIC MEASUREMETS IN THE POST-HOLE COVOLUTE OF SADIA'S Z-MACHIE (IVITED)" PPC 978-1-4577-0631-8/11 2011 IEEE

25. B. Jones, D. S. Nielsen, L. B. Nielsen-Weber, J. D. Serrano, C. J. Meyer, C. A. Coverdale,D. J. Ampleford, C. A. Jennings, S. B. Hansen, M. E. Cuneo, J. P. Apruzese, R. W. Clark, P. L. Coleman "Multi color gated x-ray pinhole imaging of z-pinch implosions on the Saturn and Z pulsed power generators" Presented ICOPS 2011

26. B.Jones, Coverdale, Christine A.; Cuneo, Michael E.; Savage, Mark E.; Davis, Jack L.; Jones, S.C.; Jennings, Christopher Ashley; Stygar, William A.; Jones, Michael C.; LeChien, Keith R.; Thornhill, J. W.; Giuliani, J. L.; Clark, Robert W.; Chong, Young K.; Chittenden, Jeremy P.; Ampleford, David J.; Waisman, Eduardo M.; Apruzese, John P.; Whitney, Kenneth G.; Dasgupta, Arati "Large diameter copper wire array implosions for K-shell x-ray generation on the refurbished Z machine" Presented ICOPS 2009

27. MICHAEL JONES, DAVE AMPLEFORD, MIKE CUNEO, CHRIS JENNINGS, BRENT JONES, MIKE LOPEZ, GREG ROCHAU, MARK SAVAGE, JOHN PORTER, "Total X-Ray Power Improvement on Recent Wire Array Experiments on the Z Machine" Presented APS-DPP 2010

28. M. R. Gomez, private communication.

29. D. J. Ampleford et al Physics of Plasmas in preparation.

APPENDIX - COUPLING OF CIRCUIT MODEL TO MHD CODE

The circuit model discussed here is applied to the resistive MHD code GORGON. A series of lumped circuit element transmission lines are coupled together through a series of convolute inductances, through to the load region. The convolute loss is applied as a resistor to ground at the connection between the A level MITL and the convolute.

A similar approach was previously attempted to model the implosion and stagnation of compact wire arrays on the Z generator prior to, and shorty after its recent refurbishment [4]. The details of how the equivalent circuit was created, integrated, and coupled to the load model have however been modified as discussed below, to make this approach applicable to a wider variety of loads imploded on Z.

The approach we now take is to couple the load and circuit model through a number of stages. This ensures we are able to accurately represent discrete parts of the problem, accounting for all the inductances in the system, whilst enabling us to sub cycle parts of the problem from one another to reduce computational overhead.

The discrete stages into which we divide the problem are:

MHD model of the imploding load
Short radial transmission line to start of feed
Inductance representing final feed
Transmission line coupling inductances (the convolute)
4 Radial transmission lines from water section to convolute.

Effective computational modeling of realistic loads fielded on the Z generator is complicated by the need to model the evolution of dense plasmas surrounded by large regions of vacuum. The GORGON MHD code overcomes this problem by essentially modeling the vacuum and plasma regions separately. We use an explicitly integrated electromagnetic field solver to model the propagation of electric and magnetic fields through vacuum regions, and then allow these equations to relax to a magnetic field diffusion scheme as the resistivity rises in the plasma. The use of an explicit integration scheme makes the distribution of the problem over parallel computers quite trivial. Unlike more typical resistive MHD schemes in which the vacuum is modeled as a region of high resistivity, we are also able to more effectively exclude current from vacuum regions. We do however have to operate on small time steps dictated by the speed of light transit time across a computational zone. Because of this we typically sub cycle the field solver on a smaller time step than that set by the hydrodynamics, so as to reduce the runtime of our calculations. We apply boundary conditions by setting the magnetic field at a certain radius, then integrating the electric field at that radius to recover the voltage. Once set electromagnetic waves may propagate the field across the vacuum to the plasma. The circuit model we use to supply the current and set the magnetic field at the boundary must be able to respond to the changing voltage at the same boundary location, so has to be sub cycled with the field solver. This requirement means that care must be taken to ensure the runtime of the calculation is not significantly increased. It is for this reason that the circuit model we apply is separated into stages.

Given the plasmas we implode are typically surrounded by vacuum the first, short radial transmission line we couple to the computational volume has to couple to this vacuum region. The electromagnetic field solver we use is a standard leap-frog wave equation integration scheme. Given the 3D problems we typically model, we set the magnetic field and monitor the voltage on a circular boundary surrounding the problem. To reduce our computational volume we set this boundary at as small a radius as the problem will allow. The first radial transmission line we couple into therefore serves two purposes. Firstly, it azimuthally averages any variation to the fields surrounding the problem to form a single transmission line. Secondly, it enables us to extend our solution domain out in radius, to ensure we always couple to the rest of the circuit model at the same radial location. Since this line is 1D, little computational overhead is incurred, and it provides a simple way to ensure all inductances are properly accounted for by standardizing the circuit model coupling location, while allowing the MHD boundary to vary.

This short radial feed section connects to an inductor representing the feed connecting the convolute to the load, which then connects to the convolute coupling inductances. All these sections are sub cycled with the field solver, using the same leapfrog integration scheme applied to the electromagnetic field integration. The 4 transmission lines that connect to the convolute are then implicitly integrated on the time step set by the hydrodynamics.

DISTRIBUTION

1	MS 1106	C.A. Jennings	1644
1	MS 1106	D.J. Ampleford	1643
1	MS 1193	B. Jones	1643
1	MS 1193	R.D. McBride	1648
1	MS 1196	J.E. Bailey	1677
1	MS 1192	M.C. Jones	1674
1	MS 1193	M.R. Gomez	1643
1	MS 1193	M.E. Cuneo	1643
1	MS 1186	C. Nakhleh	1644
1	MS 1196	W.A. Stygar	1671
1	MS 1194	M. Savage	1671
1	MS 1189	D.G. Flicker	1646
1	MS0899	Technical Library	9536 (electronic copy)
1	MS0359	D. Chavez, LDRD Office	1911

Sandia National Laboratories